The Pennsylvania State University

The Graduate School

College of Engineering

NEXT GENERATION REACTOR CORE ANALYSIS USING ITERATIVE TRANSPORT-DIFFUSION METHODOLOGY

A Thesis in

Nuclear Engineering

by

Daniel R. Beacon

© 2014 Daniel R. Beacon

Submitted in Partial Fulfillment
of the Requirements
for the Degree of

Master of Science

August 2014

The thesis of Daniel R. Beacon was reviewed and approved* by the following:

Kostadin N. Ivanov
Distinguished Professor of Nuclear Engineering
Thesis Adviser

Maria Avramova
Assistant Professor of Nuclear Engineering

Boyan D. Ivanov
Principal Engineer
Westinghouse Electric Company, LLC
Special Signatory

Karen A Thole
Department Head of Mechanical and Nuclear Engineering

*Signatures are on file in the Graduate School.

ABSTRACT

This thesis details the efforts, changes, and improvements that have been made to the Next Generation Method (NGM) Iterative Transport-Diffusion Methodology (ITDM), a long term joint project between The Pennsylvania State University (PSU) and Westinghouse Electric Company. Significant changes to the calculation models have been made including an update to moderator properties and a completely new MCNP6 reference simulation to use for comparison to the ITDM results. However, the axial tilt seen in the previous ITDM results has remained. The cause of the tilt has been under investigation since.

Many studies have been performed covering topics such as NEM mesh sizes, PARAGON radial discretization, the B1 approximation, and inter-layer axial leakage. It was found that the B1 approximation, used to adjust for the critical neutron spectrum, had the most significant effect on the axial reaction rate distribution. However, this effect was not consistent between cases and it was decided that the B1 approximation should not be used.

The results of the original axial leakage study suggested that there was an issue with the original implementation of the axial leakage routine in the code. Upon investigation, it was found that the energy treatment in the axial leakage routine needed to be updated. This effort is currently in progress as of the writing of this thesis. Specifically, the fine group energy structure for the axial leakage source is to be reconstructed using the previous iteration energy spectra. It is hoped that this change will lead to improved axial results.

TABLE OF CONTENTS

LIST OF FIGURES vi
LIST OF TABLES viii
ACKNOWLEDGEMENTS x
CHAPTER 1 Introduction 1
CHAPTER 2 Literature Review 3
2.1 Iterative Methodologies 5
2.2 DeCART 9
2.3 MPACT 11
CHAPTER 3 Background 13
3.1 History of ITDM 13
3.2 Methodology 15
3.2.1 ITDM Methodology 15
3.2.2 PARAGON Methodology 17
3.2.3 NEM Methodology 19
3.2.4 MCNP Methodology 20
3.3 Benchmark Description 23
3.4 SNA and MC Conference Paper 28
3.4.1 Abstract 28
3.4.2 Introduction 28
3.4.3 Methodology 29
3.4.4 Application 31
3.4.5 Results 32
3.4.6 Conclusion 41
3.5 Overview of Thesis Contributions 42
CHAPTER 4 Initial Status and Preliminary Updates 43
4.1 Initial Status and Reproduction of Previous Results 43
4.2 Moderator Density Update 47
4.3 MCNP6 Temperature Update 52
CHAPTER 5 Axial Power Tilt Studies 55

5.1 NEM Discretization Study 55
5.2 PARAGON Discretization Study 61
5.3 B1 Approximation Study 66
5.4 Axial Leakage Study 74
5.5 Axial Leakage Energy Reconstruction 81
5.6 Diffusion Coefficient Energy Collapsing 84
CHAPTER 6 Conclusions and Future Work 85
6.1 Conclusions 85
6.2 Future Work 88
APPENDIX A List of Files 89
APPENDIX B Results Instructions 91
REFERENCES 92

LIST OF FIGURES

Figure 1: ITDM Iteration Scheme (Colameco D. , 2012) 16

Figure 2: C3 Radial Assembly Arrangement 23

Figure 3: C5 Radial Assembly Arrangement (Colameco, Ivanov, Beacon, & Ivanov, 2013) 24

Figure 4: C5 Axial Control Rod Configurations (Colameco D. , 2012) 25

Figure 5: Uranium Oxide (UOX) Fueled Assembly Composition 26

Figure 6: Mixed Oxide (MOX) Fueled Assembly Composition 27

Figure 7: ITDM Depletion Scheme 31

Figure 8: PARAGON-MCNP Model Iterations 37

Figure 9: 3D C3 ARO MCNP Convergence 38

Figure 10: 3D C3 ARO MCNP Axially Homogeneous Core Flux Convergence 39

Figure 11: 3D C3 Core Fission Reaction Rate Shape 40

Figure 12: C3 ARO NW UOX Assembly Reproduction of Results 44

Figure 13: C3 ARO NE MOX Assembly Reproduction of Results 45

Figure 14: C3 ARO Core Average Reproduction of Results 45

Figure 15: C3 ARO NW UOX Assembly Density Update Comparison 49

Figure 16: C3 ARO NE MOX Assembly Density Update Comparison 50

Figure 17: C3 ARO Core Average Density Update Comparison 50

Figure 18: C3 ARO NW UOX Assembly Temperature Update Comparison 53

Figure 19: C3 ARO NE MOX Assembly Temperature Update Comparison 53

Figure 20: C3 ARO Core Average Temperature Update Comparison 54

Figure 21: C3 ARO NW UOX Assembly NEM Axial Mesh Comparison 55

Figure 22: C3 ARO NE MOX Assembly NEM Axial Mesh Comparison 56

Figure 23: C3 ARO Core Average NEM Axial Mesh Comparison 56

Figure 24: C3 ARO NW UOX Assembly NEM Radial Mesh Comparison..... 57

Figure 25: C3 ARO NE MOX Assembly NEM Radial Mesh Comparison 58

Figure 26: C3 ARO Core Average NEM Radial Mesh Comparison..... 58

Figure 27: Paragon Radial Discretization Levels: No, Low, and High respectively..... 61

Figure 28: C3 ARO NW UOX Assembly PARAGON Discretization Comparison 62

Figure 29: C3 ARO NE MOX Assembly PARAGON Discretization Comparison..... 62

Figure 30: C3 ARO Core Average PARAGON Discretization Comparison 63

Figure 31: C3 ARO NW UOX Assembly B1 Comparison 67

Figure 32: C3 ARO NE MOX Assembly B1 Comparison..... 67

Figure 33: C3 ARO Core Average B1 Comparison 68

Figure 34: C3 RA HZP NW Rodded UOX Assembly B1 Comparison 70

Figure 35: C3 RA HZP SE UOX Unrodded UOX Assembly B1 Comparison..... 70

Figure 36: C3 RA HZP NE MOX Assembly B1 Comparison 71

Figure 37: C3 RA HZP Core Average B1 Comparison..... 71

Figure 38: C3 ARO NW UOX Inter-Layer Axial Leakage Comparison 75

Figure 39: C3 ARO NE MOX Inter-Layer Axial Leakage Comparison..... 75

Figure 40: C3 ARO Core Average Inter-layer Axial Leakage Comparison..... 76

Figure 41: C3 ARO NW UOX Assembly Axial Leakage with NEM Discretization..... 78

Figure 42: C3 ARO NE MOX Assembly Axial Leakage with NEM Discretization 79

Figure 43: C3 ARO Core Average Axial Leakage with NEM Discretization..... 79

LIST OF TABLES

Table 1: 2D C3 ARO ITDM to PARAGON K_{eff} and Assembly Fission RR Differences 33

Table 2: 2D C3 ARO ITDM to PARAGON Pin Differences..... 33

Table 3: 2D C3 Rodded-A ITDM to PARAGON Keff and Assembly Fission RR Differences.. 33

Table 4: 2D Rodded-A ARO ITDM to PARAGON Pin Differences..... 34

Table 5: 2D C3 Rodded-B ITDM to PARAGON Keff and Assembly Fission RR Differences.. 34

Table 6: 2D C3 Rodded-B ITDM to PARAGON Pin Differences..... 34

Table 7: ITDM depletion results for the 2D 2x2 C3 Un-Rodded mini-core problem 35

Table 8: 3D C3 ARO ITDM to MCNP Assembly Differences 39

Table 9: C3 ARO Core Average Multiplication Factor Reproduction of Results..... 46

Table 10: Moderator Properties by Layer with MCNP5 Temperatures 48

Table 11: C3 ARO Core K_{eff} Density Update Comparison 51

Table 12: C3 ARO Core K_{eff} Temperature Update Comparison 54

Table 13: C3 ARO Core K_{eff} NEM Discretization Comparison..... 59

Table 14: C3 ARO Pin Power Errors MCNP6 vs. ITDM 1NPA..... 59

Table 15: C3 ARO Pin Power Errors MCNP6 vs. ITDM PxP 60

Table 16: C3 ARO Core K_{eff} PARAGON Discretization Comparison 63

Table 17: C3 ARO Pin Power Errors MCNP6 vs. ITDM High..... 64

Table 18: C3 ARO Pin Power Errors MCNP6 vs. ITDM Low 64

Table 19: C3 ARO Pin Power Errors MCNP6 vs. ITDM No..... 64

Table 20: C3 ARO Core Average K_{eff} B1 Comparison 69

Table 21: Control Rod Material Composition 69

Table 22: C3 RA HZP Core K_{eff} B1 Comparison..... 72

Table 23: C3 RA HZP Pin Power Errors MCNP6 vs. ITDM B1 off..... 72

Table 24: C3 RA HZP Pin Power Errors MCNP6 vs. ITDM B1 on 73

Table 25: C3 ARO Core Average K_{eff} Inter-Layer Axial Leakage Comparison..... 76

Table 26: C3 ARO Pin Power Errors MCNP6 vs. ITDM No AL 77

Table 27: C3 ARO Pin Power Errors MCNP6 vs. ITDM AL 77

Table 28: C3 ARO Core Average K_{eff} Axial Leakage NEM Discretization Comparison..... 78

Table 29: Accompanying Files 89

ACKNOWLEDGEMENTS

I would like to thank Westinghouse Electric Company, LLC for supporting this project through its duration, and also the Nuclear Regulatory Commission for supporting me personally during my studies at Penn State.

I would also like to thank my adviser, Dr. Kostadin Ivanov, mentor, Dr. Boyan Ivanov, and Dr. David Colameco for contributing their expertise, knowledge and help during the continuation of work on this project.

Finally, I would like to thank my parents, George and Roxanne, and my sister, Kelly, for their support and guidance throughout not only my academic career, but my entire life.

CHAPTER 1
INTRODUCTION

The nuclear power industry faces many challenges. Of the utmost importance, safety is one of these challenges and is focused on in every design. Additionally, next generation designs seek to improve the efficiency and cost effectiveness of the reactor. The combination of these fundamental design bases leads to many non-fundamental designs. The ever-increasing complexity of new nuclear reactor designs, combined with the growing capabilities of computer processing, create both the necessity, and the means, for high-fidelity multi-group three-dimensional (3-D) heterogeneous transport-accurate core wide simulations. Traditional methods relying solely on diffusion approximation techniques and once through processes that use pre-calculated environmentally insensitive few-group cross section libraries are becoming outdated and are proving to be insufficient to meet the goals of next generation designs.

The purpose of the Iterative Transport-Diffusion Methodology (ITDM) presented in this thesis is to provide the desired full core simulation with 3-D transport-accuracy while keeping computing requirements reasonable. The iterative nature of the program is required to reduce computational costs since 3-D full core transport solutions are still currently too computationally intensive for practical use.

The Iterative Transport-Diffusion Method is a long term joint project between The Pennsylvania State University (PSU) and Westinghouse Electric Company. It uses an embedded transport approach that is expected to provide results with near 3D transport accuracy for a fraction of the time required by a full 3D transport method. It could be viewed as a 3D whole core heterogeneous transport calculation consisting of a large number of local heterogeneous solutions that are coupled together by partial currents in order to obtain the global heterogeneous solution. This approach aims to avoid any changes to the underlying transport and nodal solvers

in order to maintain the portability of the methodology. (Colameco, Ivanov, Beacon, & Ivanov, 2013)

Chapter 2 of this thesis will explore the state of the industry with regards to next generation iterative methodologies. It will cover a range of other projects similar to ITDM. Next, Chapter 3 will give an in depth background of the ITDM project, beginning with a brief history. It will go on to explain the methodologies and benchmark cases in ITDM, and then give an overview of the main contributions of this thesis. It also includes a conference paper that gives a concise summary of the project up to the starting point of this thesis's contributions.

Chapter 4 will then describe the starting point and necessary preliminary updates required for the ITDM project. The bulk of the thesis, in Chapter 5, details the investigation of an axial tilt phenomenon seen in ITDM results. It contains a number of studies designed to systematically pinpoint the cause of the axial tilt seen. Finally, in Chapter 6, conclusions are drawn and a path forward for the project is suggested.

CHAPTER 2
LITERATURE REVIEW

The traditional neutronics core design and safety simulation, currently used in nuclear industry and regulation, is performed on assembly scale (level). For deterministic neutronics methods the recent advances and developments in reactor design and safety analysis towards more physics-based high-fidelity simulations include replacing two group diffusion neutronics solvers with multi-group transport solutions. Recently, investigations have been carried by many organizations on feasibility and importance of performing core calculations on homogenized pin level and even on within pin heterogeneity level. Such refined simulations are performed in two ways: direct and embedded (utilizing iterative methodologies). The embedded iterative calculations are more efficient and lead to reasonable calculation times but one has to take care to avoid convergence problems. Usually the embedded calculations at different levels are performed iteratively and the results of each are used to correct the boundary conditions at the other level in next iteration. At this stage of computer technology performing multi-group 3-D heterogeneous transport core calculations in direct manner is still a challenging task although there are such attempts with Method of Characteristics (MOC). Most of direct calculations are performed on homogenized pin level and using energy group structures between 4 to 20 energy groups. The utilized methods are usually diffusion, SP_N (Simplified P_N) and S_N (Discrete Ordinates). The requirement in these calculations is pre-generation of group cross-section libraries homogenized on pin-level supplemented with correction parameters such pin discontinuity factors or SPH (Super-Homogenization) factors. The selection of appropriate energy-group structure is a challenge for this approach since different calculations may require different energy-group structures. From the above discussion is clear that the iterative manner of performing multi-group 3-D heterogeneous transport core calculations is an attractive alternative

to the direct approach. In this chapter different iterative (embedded) methodologies proposed elsewhere will be discussed in order to contrast them to the methodology being developed at the Pennsylvania State University (PSU), which is unique and innovative and which is the subject of this thesis's research.

2.1 Iterative Methodologies

The ITDM project is not alone in its efforts to achieve high fidelity 3D core calculations using iterative methodologies. In a similar effort, HELIOS, a method of characteristics (MOC) lattice physics code, and INSTANT, a core simulator, are being coupled by A. Rubin in his PhD studies at Penn State for High-Temperature Reactor (HTR) calculations. This project is similar to ITDM in the fact that the lattice code performs pin cell calculations and passes online cross sections to the core simulator, which calculates a core wide solution. The difference is that the lattice calculation is performed by HELIOS-2.0 using MOC and the core calculation is based on a few-group transport method (P_N method in INSTANT). Although the coupling scheme used in this work (named Iterative Transport Transport Methodology – ITTM) has some similarity with the coupling scheme used in ITDM there are significant differences based on different methods used for core and lattice calculations in the ITTM. Also in ITTM super-homogenization techniques and SPH factors are being used. This effort is currently under way as of the writing of this thesis. (Karriem, Ivanov, Rabiti, & Gougar, 2014)

Another project at The Pennsylvania State University, demonstrated the benefits of an online cross section generation scheme (that is similar to what ITDM uses) for Fast Gas Reactor applications. This Iterative Diffusion-Diffusion Methodology (IDDM) "minimizes the inconsistency and inaccuracy in determining physics parameters by feeding actual reactor core conditions into the cross section generation process." As part of the project, a 2-D pin by pin lattice code called NEMA was developed. The code develops lattice parameters using the embedded MICROX-2 cross sections and NEM. The NEMA code was benchmarked and validated using a Monte Carlo code, SERPENT. The IDDM methodology was then tested when NEMA was used to generate online cross sections for a nodal solver, DIF3D. The results from

DIF3D were then examined and showed that the IDDM methodology improved the eigenvalue and power distribution predictions. (Hou, Ivanov, & Choi , 2014)

Researchers from the School of Nuclear Science and Technology at Xi'an Jiaotong University in China have been working on a code that couples a matrix method of characteristics (MMOC) technique in two dimensions with a 1-D diffusion based nodal expansion method. The MMOC technique uses a response matrix constructed between the source and flux using a single sweep. Additionally, geometric divisions and long characteristics are determined through an adaptation of the commercial AutoCAD code. The resulting system of linear equations is then solved iteratively using a generalized minimal residual method. This technique was compared to traditional MOC calculations in 2-D C5G7 benchmark tests and showed that accuracy is maintained, while reducing the computational time. The 2-D MMOC results are then coupled, through the transverse leakages, to the 1-D diffusion calculation and the neutron balance is achieved using a 3-D course mesh finite difference (CMFD) calculation. In the 3-D C5G7 benchmark tests, it is seen that the coupling scheme achieves acceptable accuracy in comparison to the reference solution with a CPU time of approximately 12 hours and a memory usage of 2GB. (Zhang, Zheng, Wu, & Cao, 2013)

Researchers at EDF in France are developing a code, MICADO, which combines 2-D MOC calculations with a 1-D axial transport calculation. The 1-D calculation provides a set of axial leakage source terms that are used to couple the individual 2-D slices of the problem. Emphases in the studies were placed on convergence and parallel computing efficiency in the code. It was found that the application of the coupling scheme did not affect the spatial convergence order of the MOC solver, though drawbacks were seen regarding the storage of axial leakage source terms between iterations. Regarding the parallel computing efficiency, it

was found to be acceptable, but was noted that the code could be improved using SIMD instructions. (Fevotte & Lathuiliere, 2013)

Another similar effort is being made at Osaka University in Japan. In this methodology, a 2-D method of characteristics lattice physics code (GALAXY) is coupled with a 3-D S_N nodal solver (TECHXY). This methodology also uses SPH factors in addition to the cross sections when passing information to the nodal solver. SPH factors are ratios between the MOC calculated volume averaged heterogeneous fluxes and the assembly averaged homogenized fluxes and are used to preserve the flux shape distribution. In their work, a comparison to the traditional once through off-line approach was made. It was seen that the pin-wise maximum power difference had decreased, however a slight increase in error was seen in the K_{eff} prediction. (Takeda, Fujita, Kitada, Yamaji, & Matsumoto, 2009)

A project at the Korea Advanced Institute of Science took a slightly different approach. A 2-D MOC code is also used. However, it is coupled with a 1-D S_N like calculation that uses the generated cross sections to calculate an axial distribution. This axial flux is then used in the MOC calculation as an additional source in the neutron balance equation. Similarly, the radial fluxes are used as sources in the 1-D transport calculation. The team improved upon this method, though, by using a linear characteristic method in 1-D rather than the S_N like approach. (Lee & Cho, 2006)

Researchers at Seoul National University in Korea have developed a code called nTRACER. The code uses 2-D planar MOC calculations coupled with 3-D CMFD calculations and employs surface currents and cell average fluxes between iterations. The axial solution is obtained through an SP_3 calculation. This project further extends its capabilities, though, by adding depletion and coupling the nTRACER program to a thermal hydraulics code for

feedback. The program has been benchmarked using simulations of ORP1000 cores. It was shown to be capable of "subpin level flux, temperature, and isotopic inventory calculation incorporating detailed thermal feedback and depletion effects." It was concluded that "direct whole core calculation without any prior calculations or adjustments is possible to produce very accurate and detailed information throughout the cycle with the nTRACER approaches for practical high-fidelity simulations." (Jung, Joo, & Yoon, 2013)

2.2 DeCART

A group of researchers from the Department of Nuclear Engineering and Radiological Sciences at The University of Michigan is working on improvements to the 2D/1D coupled code called DeCART. This work is part of the Consortium for the Advanced Simulation of Light Water Reactors (CASL). DeCART is a code originally developed by the Korea Atomic Energy Research Institute (KAERI) that couples 2-D MOC/CMFD calculations with a 1-D nodal diffusion calculation. It uses axial transverse leakages to couple the two calculations, much like many other 2-D/1-D codes. However, the limits of the methodology have been pushed by researchers at The University of Michigan. The axial slices used for the 2-D MOC calculations have been thinned and adjusted to account for more detailed reactor core features, such as spacer grids. This refinement leads to instabilities in the DeCART code that were investigated by the researchers in Michigan. It was found that there were many sources of instability in the DeCART code. Some of these included negative sources and coupling coefficients. (Stimpson, Young, Collins, Kelley, & Downar, 2013)

The researchers at the University of Michigan devised multiple sets of equations to be used to remedy the issues seen in DeCART. In this work, they "systematically discretize the 2D/1D equation to obtain a system of discrete equations whose solution converges to the exact 2D/1D solution as the grid becomes increasingly fine." They also introduce an iteration method to solve this system of equations. (Kelley & Larsen, 2D/1D Approximations to the 3D Neutron Transport Equation. I: Theory, 2013)

Upon testing the introduced methodology, it was found that the iterative scheme devised was stable and performed as expected. It was compared to a full 3-D MOC transport solution for

verification using many different simple test cases. The researchers showed that the 2D/1D methodology was transport-accurate in the radial plane, and at least diffusion accurate in the axial direction. It was also discovered that the key element with regards to the stability of the iterative methodology was an "under-relaxation" step that was used. This was the defining difference between the original DeCART implementation, and the methodology developed by the researchers. It was concluded that the knowledge gathered from the DeCART code and the methodology proposed would be applied to a newer code, MPACT. (Kelley, Collins, & Larsen, 2013)

2.3 MPACT

Another group of researchers from the Department of Nuclear Engineering and Radiological Sciences at the University of Michigan are now developing a code named the Michigan Parallel Characteristics Transport Code (MPACT). This code is part of the Virtual Environment for Reactor Analysis (VERA), the end-user reactor simulation tool being produced by CASL. The MPACT code includes 2-D and 3-D MOC and 2-D and 3-D methods of collision direction probabilities (CDP) as well as detailed cross section resonance treatment. It is being developed using several modern software concepts and best practices. Currently, the code's 3-D simulations are limited to computationally intensive full 3-D transport solutions. However, parallelization and iterative 2-D/1-D schemes are also being explored and will be added to the code in the future. (Kochunas, Collins, Jabaay, Downar, & Martin, 2013)

The 2-D capabilities in MPACT have been extensively tested and verified. Cases used were the C5G7 benchmark and the VERA Core Physics Progression Problems. It was seen that the 2-D capabilities of the MPACT code have been verified and that implementation was successful. Therefore, work on implementing 3-D methodologies was approved. (Collins, Kochunas, & Downar, 2013)

Improvements to the 3-D MOC calculation used in MPACT have also been under development. Computational requirements have been reduced using a newly developed variation of the modular ray tracing technique in the 3-D transport kernel. This variation differs in the way the polar angle is determined in the ray tracing scheme. It cuts the required ray tracing information in half by using the same information for positive and negative ray tracing directions. However, spatially, the ray traces are required to be closer together, and therefore more numerous using this technique. A parallel model is being developed, though, that makes

use of both distributed and shared memory models with capabilities of decomposition in space, angle, and characteristic ray. Preliminary results for this method are promising, matching the benchmark well. (Kochunas & Downar, 2013)

Additionally, a technique was developed in MPACT that is a hybridization of the collision probabilities method (CPM) and the MOC. The technique, called characteristic detection probabilities (CDP), combines the benefits of CPM with the MOC by only coupling the fine mesh regions passed by the characteristic rays. This reduces the scale of the probabilities matrix while still maintaining the MOC's ability to deal with complicated geometries. This technique has shown to improve upon computation times when compared to the standard MOC for some cases such as the C5G7 benchmark. It was noted that larger 3-D cases showed greater benefits using the technique. However, some other problems created difficulties that are still being investigated. (Liu, Kochunas, Collins, Downar, & Wu, 2013)

CHAPTER 3
BACKGROUND

3.1 History of ITDM

This project is a continuation of efforts made by multiple individuals and is supported by the Westinghouse Electric Company. First, Dr. Boyan D. Ivanov began working on the ITDM project. His dissertation entitled *Methodology for Embedded Transport Core Calculation* outlines the initial efforts made. The challenges regarding steep gradients and reactor complexities that are faced by two-step offline calculations traditionally used for core simulations served as inspiration to develop two innovative methodologies.

The first of these methodologies consisted of embedded SP_3 Pin-by-Pin calculations in a NEM framework. This methodology greatly improved upon the old two-step offline calculations. However, the embedded SP_3 calculations "were found to have limited accuracy due to the use of pre-calculated few-group pin-wise homogenized cross-sections." Therefore, the second methodology replaced the SP_3 calculations with heterogeneous lattice calculations that used collision probability and online cross-section generation through the equivalence theory. This eliminated many of the uncertainties, and consequently many of the sources of error, that were previously introduced by the off-line cross section generation methods. Many difficulties were addressed and overcome in Dr. Boyan Ivanov's work, such as spatial reconstruction of albedo boundary conditions and reflector convergence. (Ivanov, 2007)

Next, Damon Roberts contributed to the project. His work is detailed in his thesis entitled *Development of Iterative Transport – Diffusion Methodology for LWR Analysis*. In his work, the iterative embedded PARAGON-NEM methodology was finalized and tested on challenging two dimensional problems. It was found that incident partial current fixed sources could be used

rather than albedo boundary conditions. PARAGON, the collision probability based lattice code, was modified in order to accept these partial current sources as input. Before his work ended, Roberts began investigating three-dimensional applications for the ITDM program. (Roberts, 2010)

The most recent work on this project was performed by Dr. David Colameco and is detailed in his dissertation entitled *Next Generation Iterative Transport-Diffusion Methodology (ITDM) for LWR Core Analysis*. Dr. Colameco extended the ITDM program to three dimensions and implemented axial leakage calculations. This was done by leaving the lattice code PARAGON in two dimensions, and extending the nodal diffusion solver, NEM, to three dimensions. The codes were loosely coupled using partial current boundary conditions. Promising radial results were seen and burn-up capabilities were also added. MCNP was used as a basis for comparison for the three dimensional cases. However, there were issues seen in cases with high heterogeneity and in the axially heterogeneous three-dimensional case. It was concluded that the polynomial flux expansion used may not be sufficient, and that a semi-analytic nodal solver should be implemented. (Colameco D. , 2012)

3.2 Methodology

3.2.1 ITDM Methodology

The ITDM program uses a 2-D transport theory solver, PARAGON, which uses the method of collision probabilities. This is coupled with a 3-D nodal core diffusion solver, NEM (nodal expansion method), that is being developed by the Reactor Dynamics and Fuel Management Group at Penn State. In ITDM, radial partial currents with angular dependence are used as incoming boundary conditions for PARAGON in addition to K_{eff} and net axial currents. Each of these parameters is generated by NEM and used by PARAGON to simulate the current state of the core in the region of interest. In this way, PARAGON can then accurately produce cross sections that reflect the specific conditions of each region being simulated. These online generated cross sections are then passed to NEM in order to produce more accurate results. This process is repeated until the partial currents converge, after which a final solution is obtained.

The code has been extended to include burn-up steps, if desired. In this case, PARAGON is run in depletion mode using the converged boundary conditions of an initial ITDM run and is used to generate new inputs. These new inputs are again run through the iteration process described above. This process can be repeated for the desired burn-up steps. Figure 1 depicts the iterative nature of the ITDM program.

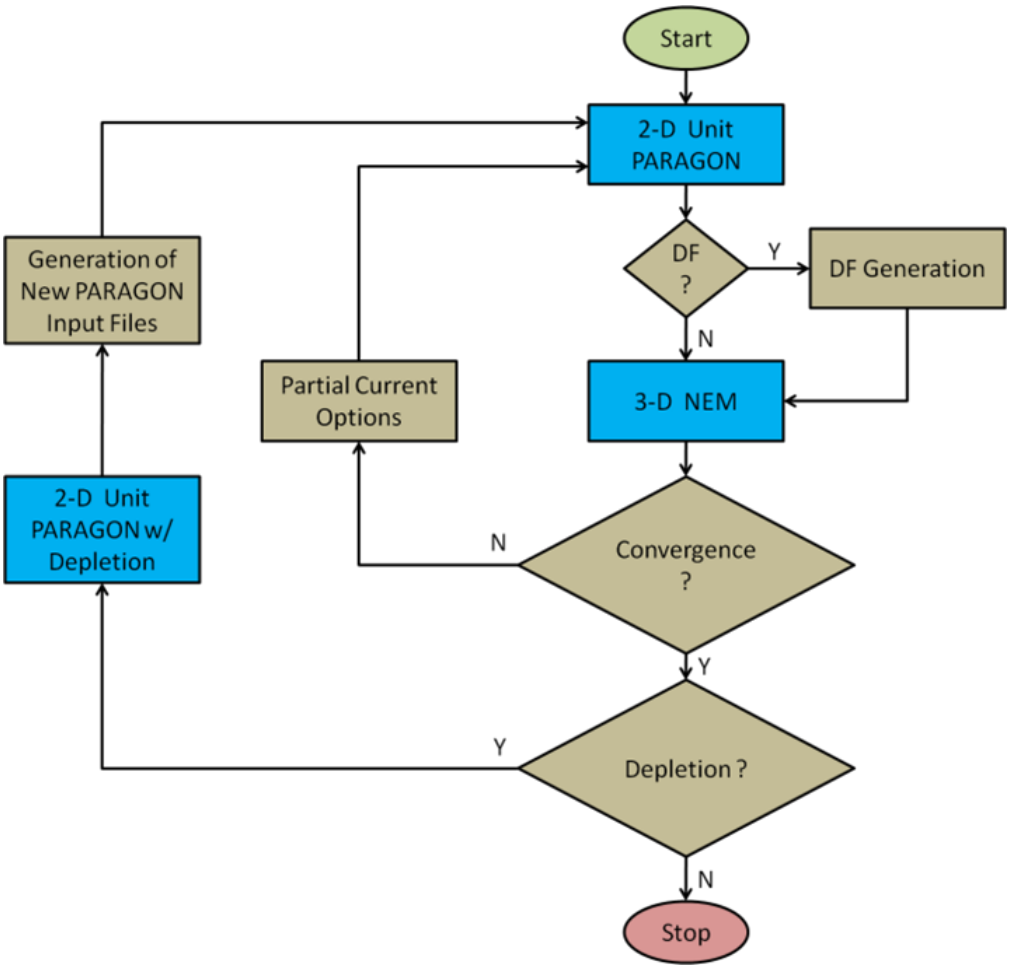

Figure 1: ITDM Iteration Scheme (Colameco D. , 2012)

3.2.2 PARAGON Methodology

PARAGON is a 2-D transport theory code developed and maintained by Westinghouse Electric Company, LLC. The method of collision probabilities, used by PARAGON, is a widely used technique for solving integral transport equations. (Lewis & Miller, 1993) In its simplest form, consider a slab geometry with domain $0 \leq x \leq a$ surrounded by vacuum with no sources. The integral scalar flux equation can then be written as: (Lewis & Miller, 1993)

$$\emptyset(x) = \int_0^a dx' \frac{1}{2} E_1[\tau(x,x')] Q(x') \tag{3.1}$$

Where the transport kernel, $E_n(\tau)$, is defined as: (Lewis & Miller, 1993)

$$E_n(\tau) \equiv \int_1^\infty \frac{d\gamma}{\gamma^n} e^{-\tau\gamma} \tag{3.2}$$

In equations (3.1) and (3.2), τ represents the optical path, γ represents the ratio of the distance traveled by the particle to the optical path, and Q represents the emission density and is approximated in equation (3.5) below. First, consider an interval, i, contained in the problem domain where: (Lewis & Miller, 1993)

$$\Delta_i \equiv x_{i+\frac{1}{2}} - x_{i-\frac{1}{2}} \tag{3.3}$$

Within this interval, it is assumed that there are no material interfaces and that cross sections are constant, except at the interfaces located at $x_{i+1/2}$ and $x_{i-1/2}$ where material interfaces and discontinuities may occur. Then, defining the average scalar flux on the interval, equation (3.4) is obtained: (Lewis & Miller, 1993)

$$\emptyset_i = \frac{1}{\Delta_i} \int_{x_{i-1/2}}^{x_{i+1/2}} dx \int_0^a dx' \frac{1}{2} E_1[\tau(x,x')] Q(x') \tag{3.4}$$

Now, the emission density is approximated using equation (3.5): (Lewis & Miller, 1993)

$$Q(x) \approx Q_i = \sigma_{si}\phi_i + S_i \tag{3.5}$$

Finally, the flux can be represented for all intervals in the domain in terms of the first flight collision probability, $P_{ii'}$: (Lewis & Miller, 1993)

$$\sigma_i \Delta_i \phi_i = \sum_{i'=1}^{I} P_{ii'} \Delta_{i'} (\sigma_{si'} \phi_{i'} + S_{i'}) \tag{3.6}$$

Where the first flight collision probability is: (Lewis & Miller, 1993)

$$P_{ii'} = \frac{\sigma_i}{\Delta_{i'}} \int_{x_{i-1/2}}^{x_{i+1/2}} dx \int_{x_{i'-1/2}}^{x_{i'+1/2}} \int_0^a dx' \frac{1}{2} E_1[\tau(x, x')] \tag{3.7}$$

This first flight collision probability may be interpreted as the probability that a neutron emitted from an isotropic unit source within interval i' will make its first collision within interval i. (Lewis & Miller, 1993) The advantage of this method is that no accuracy is lost to angular approximations, since only the collision rate is used. However, this method is limited by the fact that accuracy is truncated to the order Δ. (Colameco D. , 2012)

3.2.3 NEM Methodology

The Nodal Expansion Method (NEM) code, developed and maintained at Penn State, uses few-group nodal diffusion theory to produce three dimensional flux solutions. It has been developed in Cartesian, cylindrical, and hexagonal coordinate systems, and can accept user specified discontinuity factors.

It begins with the steady-state multi-group neutron diffusion equation and applies Fick's law. One dimensional polynomial flux expansion equations are coupled to create the relationship between the node averaged flux and the surface averaged net currents, which is required in the spatial solution for the neutron flux. In NEM, the 4^{th} order polynomial flux expansion is used, shown in equations (3.8) and (3.9) below. (Colameco D. , 2012)

$$\emptyset_z(x) = \emptyset_0 + \sum_{n=1,4} \emptyset_n f_n\left(\frac{x}{\Delta x}\right) \tag{3.8}$$

Where:

$$f_1(x) = x, \quad f_2(x) = 3x^2 - \frac{1}{4}, \quad f_3(x) = x^3 - \frac{x}{4}, \quad f_4(x) = x^4 - 3\frac{x^2}{10} + \frac{1}{80} \tag{3.9}$$

These flux expansion equations require the use of the transverse integration approximation and calculation of expansion coefficients. A step-by-step detailed description of the calculations can be found in the NEM Theory Manual. (RDFMG, 2009)

3.2.4 MCNP Methodology

The Monte Carlo N-Particle (MCNP) code is developed and maintained by Los Alamos National Laboratory (LANL). It is a general purpose Monte Carlo code with a wide range of applications. The Monte Carlo simulations used by MCNP vary significantly from those of the deterministic methods previously mentioned. In this case, statistical processes (such as nuclear particles interacting with matter) can be theoretically reproduced using random number generators (RNG). The probability distribution functions (PDF) of these processes are determined and take into account the cross sections for each possible event as well as the conditions of the problem. These PDFs can then be sampled, tallied, and statistically analyzed to describe the entire phenomenon of interest.

MCNP is found to be particularly useful for complex simulations in which many deterministic approaches cannot accurately describe the conditions or geometry due to the fact that it does not use phase space boxes and therefore does not include any space averaged values. However, obtaining highly accurate results in large simulations can prove to be computationally intensive. Therefore, many variance reduction techniques are employed in MCNP. These include truncation methods, population control methods, modified sampling methods, and partially deterministic methods. Despite these efforts, MCNP simulations still prove to be somewhat time consuming and computationally intensive. (X-5 Monte Carlo Team, 2003)

In the ITDM project, MCNP is used to generate a reference 3-D solution for direct comparison. In these reference simulations, track length tallies were used on a Pin-by-Pin (PxP) radial level and 24 layer axial level. Initially, version 5 of MCNP was used, but it was found that it lacked some of the capabilities that were desired for the simulation; specifically, temperature

dependence and chemical compound treatment. Therefore, version 6 was then used since it has been updated with these capabilities.

Specifically, MCNP6 uses a utility called "fit_otf". The utility creates new cross section sets for user specified temperature ranges by Doppler broadening the standard ENDF libraries. This is done "by interpolation using a high order functional expansion for the temperature dependence of the Doppler-broadened cross section for each isotope." (Martin, Wilderman, Brown, & Yesilyurt, 2013) This methodology has been tested and confirmed to be accurate. Additionally, the MCNP6 reference simulation uses specially generated ENDF cross section library files that account for the chemical composition of the moderator, rather than treating the moderator as a free gas. These cross section libraries are called "lwtr" libraries and have also been adjusted for the specific temperature requirements of the reference simulation.

Statistically, for the reference MCNP solutions in this thesis, 8000 cycles containing 150000 particles per cycle were run in each assembly. This led to a core k_{eff} standard deviation of only 2 pcm and pin-wise track length estimated flux R values of less than 0.005. These R values are calculated in MCNP using equation (3.10) below and can be used to determine the reliability of the acquired results. (X-5 Monte Carlo Team, 2003)

$$R = \frac{S_{\bar{x}}}{\bar{x}} \tag{3.10}$$

Where S is the square root of the sample variance and $\bar{x}$ is the sample mean.

Statistically, an R value of less than 0.05 is considered to be very precise and is even accurate enough for point detector simulations. (X-5 Monte Carlo Team, 2003) Therefore, we

can be certain that the reference simulations used to compare ITDM runs, with R values below 0.005, are reliable and accurate for the presented conditions.

3.3 Benchmark Description

The benchmark problems, simulated in both MCNP and ITDM, which are used for comparison are an adaptation from the C5G7 benchmark problem. The simulation consists of four 17x17 PWR assemblies: two mixed oxide (MOX) fueled and two uranium oxide (UOX) fueled. These assemblies are staggered in a 2x2 mini-core. This mini-core is simulated using 2 different radial treatments. The first, C3, is shown in Figure 2. In this arrangement the mini-core is simply surrounded by reflective boundary conditions (BC).

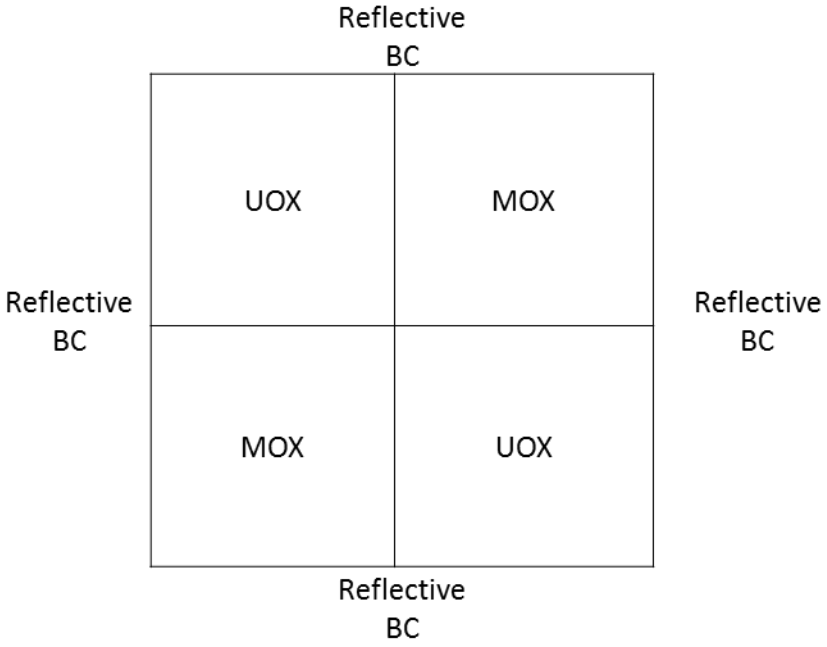

Figure 2: C3 Radial Assembly Arrangement

The other arrangement, C5, is shown in Figure 3 below. In this arrangement, the mini-core is surrounded by moderator with vacuum boundary conditions on the south and east sides. The north and west sides retain the reflective boundary conditions.

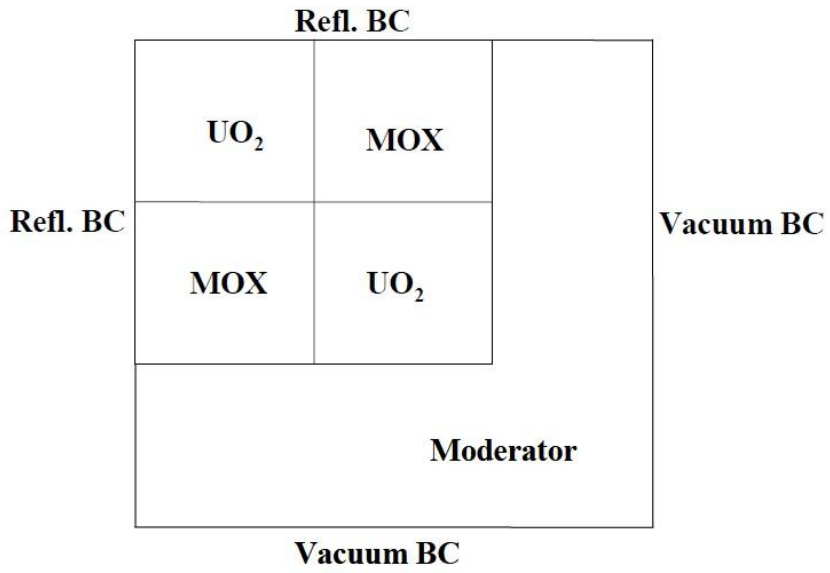

Figure 3: C5 Radial Assembly Arrangement (Colameco, Ivanov, Beacon, & Ivanov, 2013)

Axially, the 385.56 cm long core is divided into six regions with varying moderator properties. Each of these regions is then subdivided into nodes for the simulation, depending on the desired number of layers. Figure 4 shows the configuration for a 24 layer case. For each of the cases, C3 and C5, there are three different control rod configurations. The first, un-rodded, is self-explanatory. The second, rodded A, contains control rod material inserted in the guide tubes of the NW assembly as shown in the rodded A schematic in Figure 4. The third, rodded B, inserts the control rods further into the NW assembly, as shown in the rodded B configuration. It also inserts control rod material into the SW MOX assembly as shown in the rodded A configuration in Figure 4. It is important to note that the C3 cases are identical to the C5 cases depicted in Figure 4, with the exception that the C3 cases do not contain the top and bottom reflector regions. Instead, the C3 cases use reflective boundary conditions on the top and bottom of the core.

For the 2-D C3 and C5 rodded cases, the rodded layers of the core are simulated, with rodded A representing the case with control rod material in the guide tubes of the NW assembly,

and rodded B representing the case with both the NW and SW assemblies rodded. The majority of the work in this thesis uses the 3-D C3 un-rodded (C3 ARO) case at hot full power (HFP).

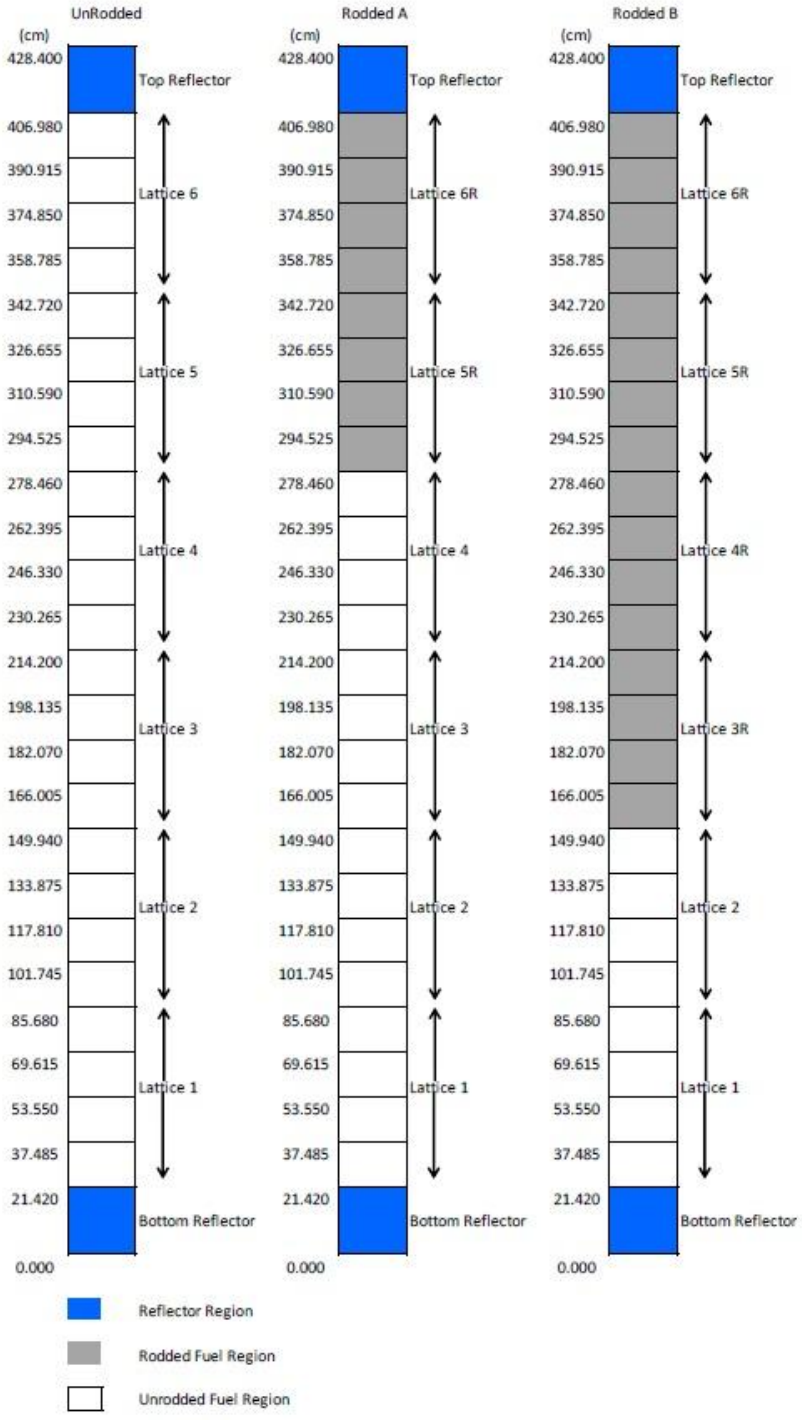

Figure 4: C5 Axial Control Rod Configurations (Colameco D. , 2012)

Each assembly consists of 289 pins in a 17x17 configuration. 25 of these pins are guide tubes which are either filled with moderator or control rod material, depending on the case. The enrichment in the UOX assemblies is constant throughout. However, the MOX assemblies contain three different fuel enrichments. Assembly compositions for each can be seen in Figure 5 and Figure 6, below.

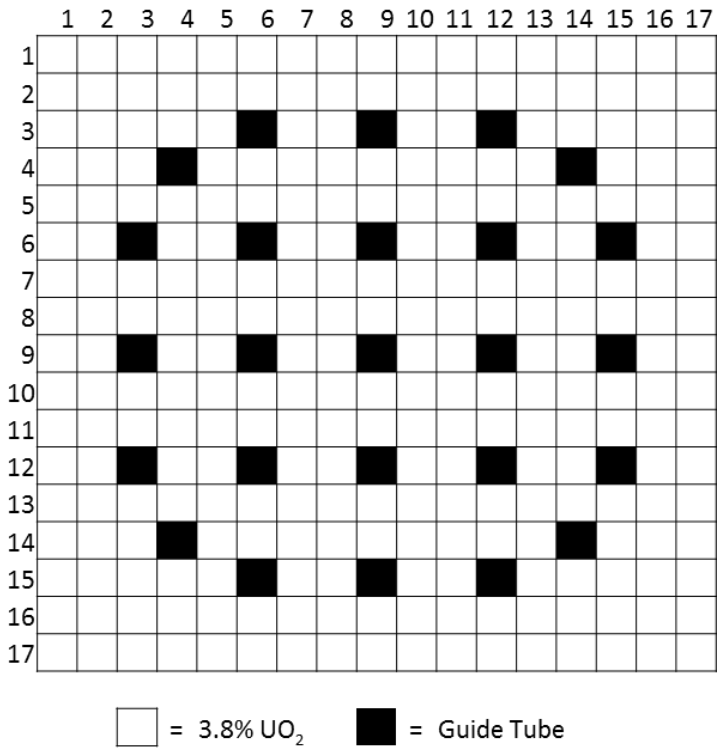

Figure 5: Uranium Oxide (UOX) Fueled Assembly Composition

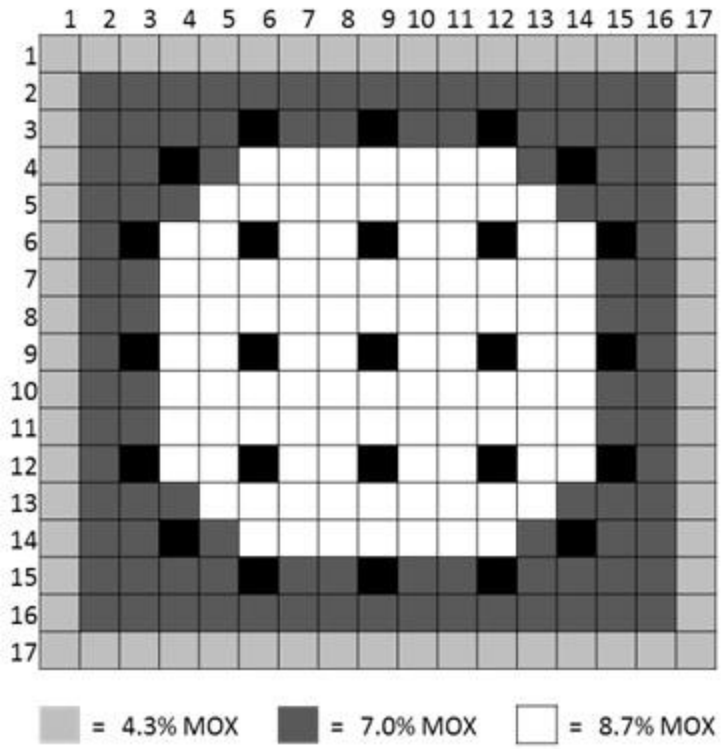

Figure 6: Mixed Oxide (MOX) Fueled Assembly Composition

3.4 SNA and MC Conference Paper

Near the beginning of the contributions of this thesis, a paper was written to summarize the current status of the ITDM project and the results up to that point and was presented at the Joint International Conference on Supercomputing in Nuclear Applications and Monte Carlo (SNA+MC) in Paris, France. Since it gives a precise overview of the project, including a summary of the background, simulations, and results, it has been included here. (Colameco, Ivanov, Beacon, & Ivanov, 2013)

3.4.1 Abstract

This paper presents an update on the development of an advanced methodology for core calculations that uses local heterogeneous solutions for on-the-fly nodal cross-section generation. The Iterative Transport-Diffusion Method is an embedded transport approach that is expected to provide results with near 3D transport accuracy for a fraction of the time required by a full 3D transport method. In this methodology, the infinite environment used for homogenized nodal cross-section generation is replaced with a simulated 3D environment of the diffusion calculation. This update focuses on burnup methodology, axial leakage and 3D modeling.

3.4.2 Introduction

This work focuses on development of one of the approaches to next generation methodology which is expected to be practical using even today's computing power for reference solutions and, in the future, for design calculations. The Iterative Transport-Diffusion Method (ITDM) is an embedded transport approach that is expected to provide results with near 3D transport accuracy for a fraction of the time required by a full 3D transport method. It could be viewed as a 3D whole core heterogeneous transport calculation consisting of a large number

of local heterogeneous solutions that are coupled together by partial currents in order to obtain the global heterogeneous solution.

This approach aims to avoid any changes to the underlying transport and nodal solvers in order to maintain the portability of the methodology. In addition to code changes it is also desirable to maintain the current level of spatial refinement in modeling. In other words there is a strong benefit to maintaining the methodology of the underlying codes. Typically in industry, cross sections are generated on a lattice level and then utilized in a nodal solver. A methodology that can use pre-existing modeling input that includes not only spatial discretization but also energy group discretization is a goal of this methodology.

3.4.3 Methodology

This development is a continuation of previous work done at 2D level utilizing the same codes but with different boundary conditions and at 3D level where partial currents were utilized in Iterative Diffusion-Diffusion Methodology (IDDM). The ITDM methodology utilizes the 2D transport code PARAGON, which is based on collision probabilities and the 3D nodal diffusion code NEM. This methodology uses incoming partial currents as radial boundary conditions to PARAGON with added characteristic of angular dependence. In addition to the radial partial current boundary conditions and the eigenvalue of the NEM solution, the axial net currents are utilized by PARAGON to define axial leakage in fixed source calculations. PARAGON is a 2D code designed to model lattices in the radial plane; output contains data for the radial surfaces and nodal averages. To approximate the PARAGON axial surface fluxes and currents, a diffusion approximation is undertaken instead of performing an additional PARAGON 1D calculation in the axial direction.

To summarize the methodology, as a first iteration, a standard one step calculation is performed where PARAGON performs lattice criticality calculations using infinite lattice boundary conditions and a 3D diffusion solution is obtained. ITDM then continues by utilizing the currents and eigenvalue from the nodal solution as boundary conditions for subsequent fixed source lattice PARAGON calculations during the iterative process. New cross sections are developed by PARAGON followed by preparation of a new set of side-dependent discontinuity factors, and a new 3D nodal diffusion solution is produced. Additional PARAGON calculations prior to the nodal solution can be undertaken to allow PARAGON to iterate over the partial currents with its neighbors. In either case, convergence is measured based on the delta of fuel node radial partial currents in the 3D nodal solution. The partial currents from the nodal solution are generated in coarse energy group and coarse spatial mesh as an average value of each side of the lattice. Before the partial currents are applied in the lattice calculation they are converted to fine energy group and fine mesh and angle based on the partial current shape f evaluated from the previous lattice calculation as shown in Eq. 3.11.

$$f(x,y,z,E,\Omega)=J(x,y,z,E,\Omega)\int dx\int dE\int d\Omega J(x,y,z,E,\Omega) \qquad (3.11)$$

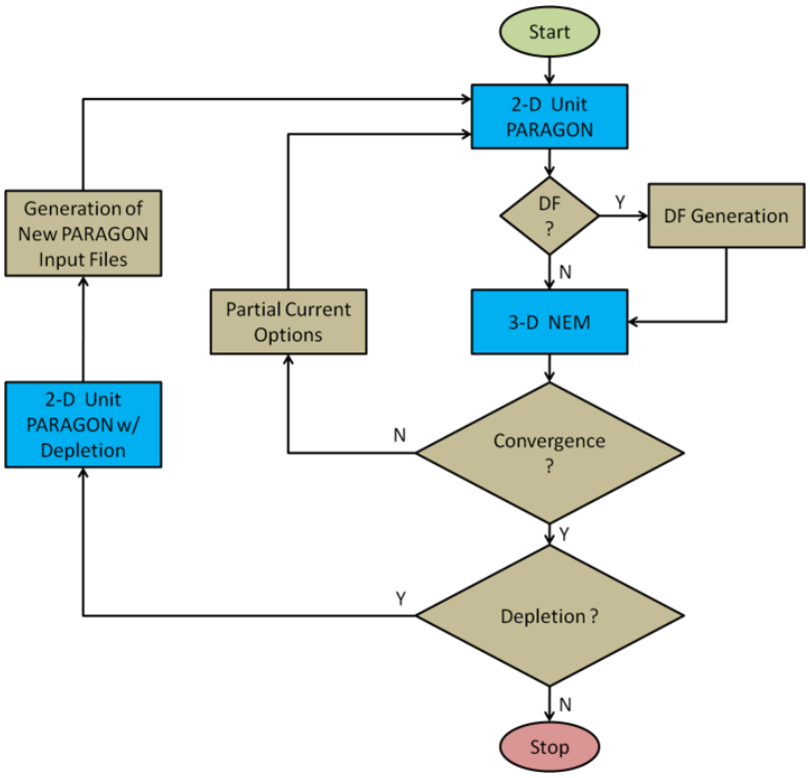

Figure 7: ITDM Depletion Scheme

The additional layer that burn-up adds to ITDM can be seen in Figure 7 above. To start, a converged solution from a set of non-linear iterations is developed using ITDM. Then a separate depletion calculation is performed lattice by lattice utilizing the boundary conditions from the converged ITDM solution. Once the depletion calculation is performed, the PARAGON inputs for the next set of ITDM iterations at the new burnup step are developed. A new full core ITDM calculation is performed utilizing the new isotopic composition from the individual lattice depletions. This process is repeated for each burnup step.

3.4.4 Application

The model used to test the burnup capability in ITDM was the C3 Un-Rodded mini-core shown in Figure 2 below. The model consists of two identical fresh UOX assemblies and two identical MOX assemblies. The UOX assembly consists of single fuel pin enrichment throughout the lattice and the MOX consists of multiple enrichments.

Three C3 2D models were developed, an un-rodded 2x2 mini-core (C3 ARO), a 2x2 mini-core with the north-west UOX assembly rodded (C3 Rodded-A), and a 2x2 mini-core with the north-west UOX and south-west MOX assemblies rodded (C3 Rodded-B). All three models had reflective boundary conditions on the outer boundaries of the model.

To test the 3D capability of the methodology the same C3 problem was used but with some modification to add axial heterogeneities like moderator density and temperature axial distributions. The axial boundary conditions are also reflective similar to radial boundary conditions.

3.4.5 Results

The C3 2D models are simulated using ITDM and are compared to the respective PARAGON heterogeneous 70-group mini-core reference solutions. PARAGON coupling order of 11 was utilized. For each of the three mini-cores the eigenvalue and assembly differences are presented first followed by the pin differences. The differences are given as absolute percent differences. The pin absolute percent differences are defined as:

$$RMS = \sqrt{\frac{\sum_N e_n^2}{N}}, \quad AVG = \frac{\sum_N |e_n|}{N}, \quad MAX = MAX(e_n), \quad MIN = MIN(e_n) \qquad (3.12)$$

where **e** is an absolute percent residual difference.

Two-group cross sections are utilized from PARAGON in NEM. The results show excellent agreement between ITDM and PARAGON. The comparisons for C3 ARO case are shown in Tables 1 and 2.

Table 1: 2D C3 ARO ITDM to PARAGON K_{eff} and Assembly Fission RR Differences

k_{eff}	Reference	1.22562	
	ITDM	1.22573	
	Difference (pcm)	11	
Fission Reaction Rate Distribution	Reference	1.1824	0.8179
	ITDM	1.1832	0.8168
	Abs. % Difference	0.08	-0.11
	Reference	0.8180	1.1817
	ITDM	0.8168	1.1832
	Abs. % Difference	-0.12	0.15

Table 2: 2D C3 ARO ITDM to PARAGON Pin Differences

	Core	NW-UOX	NE-MOX	SW-MOX	SE-UOX
MIN	-0.46	-0.14	-0.46	-0.46	-0.10
MAX	0.30	0.26	0.23	0.23	0.30
AVG	0.14	0.09	0.16	0.16	0.15
RMS	0.17	0.11	0.20	0.20	0.17

The results for Rodded-A mini-core are presented in tables 3 and 4 and also demonstrate excellent agreement between ITDM and reference predictions.

Table 3: 2D C3 Rodded-A ITDM to PARAGON Keff and Assembly Fission RR Differences

k_{eff}	Reference	1.17702	
	ITDM	1.17720	
	Difference (pcm)	18	
Fission Reaction Rate Distribution	Reference	0.4404	0.8957
	ITDM	0.4391	0.8949
	Abs. % Difference	-0.13	-0.08
	Reference	0.8959	1.7680
	ITDM	0.8951	1.7710
	Abs. % Difference	-0.08	0.29

Table 4: 2D Rodded-A ARO ITDM to PARAGON Pin Differences

	Core	NW-UOX	NE-MOX	SW-MOX	SE-UOX
MIN	-0.36	-0.36	-0.31	-0.33	-0.02
MAX	0.42	0.14	0.21	0.21	0.42
AVG	0.18	0.14	0.14	0.14	0.29
RMS	0.20	0.16	0.16	0.16	0.30

The differences for Rodded-B model are displayed in Tables 5 and 6.

Table 5: 2D C3 Rodded-B ITDM to PARAGON Keff and Assembly Fission RR Differences

k_{eff}	Reference	1.14321	
	ITDM	1.14333	
	Difference (pcm)	12	
Fission Reaction Rate Distribution	Reference	0.5653	1.0879
	ITDM	0.5645	1.0877
	Abs. % Difference	-0.08	-0.03
	Reference	0.6870	1.6598
	ITDM	0.6864	1.6614
	Abs. % Difference	-0.05	0.17

Table 6: 2D C3 Rodded-B ITDM to PARAGON Pin Differences

	Core	NW-UOX	NE-MOX	SW-MOX	SE-UOX
MIN	-0.32	-0.32	-0.16	-0.30	-0.24
MAX	0.30	0.15	0.13	0.22	0.30
AVG	0.11	0.10	0.06	0.09	0.17
RMS	0.13	0.12	0.07	0.11	0.19

The above results indicate that ITDM when utilizes the partial currents properly in fixed source lattice calculation it produces excellent results even for rodded models.

The newly developed depletion capabilities of the ITDM methodology were first tested using the 2D C3 Un-Rodded mini-core. To obtain a reference solution, the mini-core was initially depleted with PARAGON up to 41 GWd/MTU. The comparison of the ITDM depletion

to the PARAGON reference mini-core burnup calculation is excellent and shows that ITDM can accurately perform burnup steps (Table 7). The core eigenvalue is within 20 pcm and the normalized absolute pin fission reaction rate errors were less than 2% at higher burnups.

Table 7: ITDM depletion results for the 2D 2x2 C3 Un-Rodded mini-core problem

	Pin Relative Fission Reaction Rate Abs. % Errors				k-effective
Burnup	Core				Difference
GWd/MTU	RMS	AVG	MAX	MIN	pcm
0	0.11	0.1	0.21	-0.29	7
0.5	0.49	0.41	1.32	-0.81	19
1	0.32	0.29	0.66	-0.44	16
1.5	0.26	0.24	0.49	-0.41	11
2	0.21	0.19	0.41	-0.29	4
5	0.17	0.13	0.38	-0.43	-18
8	0.27	0.23	0.56	-0.58	-16
11	0.9	0.74	1.65	-1.86	-20
14	0.97	0.82	1.85	-1.94	-11
17	0.9	0.78	1.7	-1.69	-4
20	0.87	0.77	1.62	-1.54	0
23	0.68	0.62	1.28	-1.09	1
26	0.61	0.57	1.1	-0.9	-2
29	0.61	0.57	1.13	-0.85	-4
32	0.59	0.55	1.07	-0.8	-8
35	0.57	0.54	1.05	-0.78	-12
38	0.57	0.54	1.06	-0.74	-16
41	0.69	0.63	1.47	-0.82	-16

In addition to the 2D 2x2 assembly model, a larger 2D 8x8 model was developed by un-folding the 2x2 model along reflective boundaries. One burnup step was completed and the 8x8 model was compared to the corresponding PARAGON mini-core reference. The 8x8 model was further expanded axially to 24 identically layers, each 16.065 cm in height. This larger axially homogeneous 3D model has the computational space of a full size quarter core but with the ability to compare it to the 2D 8x8 and 2D 2x2 references. The results show that the 24 layer

core reproduces the 8x8 2D models and the 8x8 models reproduce the ITDM 2x2 model results. This reproduction shows that ITDM is stable for large cores.

Work is ongoing on the 3D modeling and first application was to the 3D C3 ARO case as described in Section III. While for 2D C3 cases PARAGON was used to generate the reference solutions this was impossible for the 3D case since PARAGON is 2D transport code. The Monte Carlo code MCNP with 70 energy groups is the reference of choice for this project. This is the same 70-group cross-section library used in PARAGON, which provides a consistency in the comparisons between ITDM and reference results. The MCNP lattices that comprise the 3D MCNP References model were developed iteratively from PARAGON lattices. A spatial meshing refinement was undertaken to develop consistency between PARAGON, which uses a flat flux approximation, and 70-group MCNP, which uses a continuous flux approximation. Through refining the spatial mesh by increasing the number of spatial regions, the flat flux approximation in many smaller meshes approaches the continuous treatment of the flux calculated in MCNP. These lattices were refined first and then utilized in the 3-D single assembly models and the 3-D Mini-core models. This refinement of the models at the lattice level first enables better engineering judgment of the results at the 3D level, which are comprised of those same 2D lattices. The spatial meshing refinement that was undertaken was based on an iterative method illustrated in Figure 8. If the keff differences were larger than 100 pcm or the pin differences larger than one absolute percent then spatial refinements were then made to the PARAGON model. Once the MCNP reference 3D C3 ARO model was developed it was run and converged. Figure 8 details the convergence behavior in terms of k-effective and source convergence. The results are normalized to the mean of the active cycles, cycles 1000 to 8000. The formulas for the calculations are shown below:

$$\text{Plotted Eigenvalue} = \frac{\text{Cycle Eigenvalue}}{\sum_{1001}^{8000} \text{Cycle Eigenvalue} \Big/ (8000 - 1000)} \quad (3)$$

$$\text{Plotted Source Entropy} = \frac{\text{Source Entropy}}{\sum_{1001}^{8000} \text{Source Entropy} \Big/ (8000 - 1000)} \quad (3.13)$$

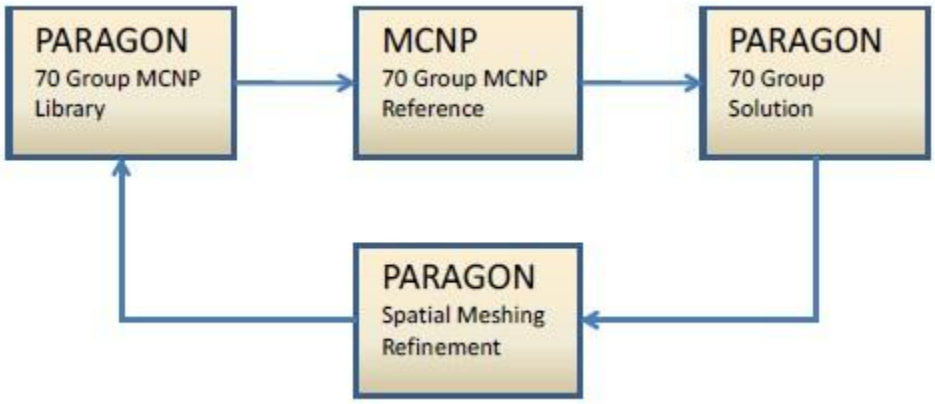

Figure 8: PARAGON-MCNP Model Iterations

The k-effective and source convergence of the 3D C3 ARO model convergence behavior is shown in Figure 9. It is what is typically seen in MCNP models - convergence takes a few hundred cycles to achieve. This 3D model has an adequate number of particles per cycle. The number of particles/cycle of 150,000 was large enough to be adequate, yet small enough to provide efficient MCNP calculations.

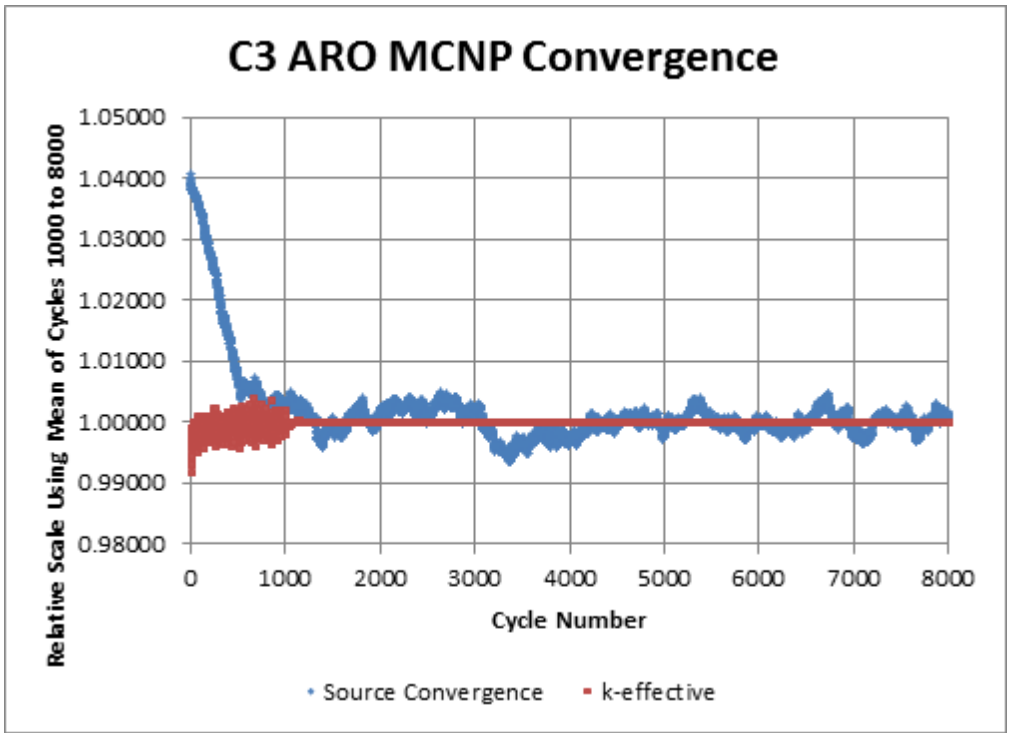

Figure 9: 3D C3 ARO MCNP Convergence

In addition the flux convergence of the MCNP 3D C3 ARO model was studied. An axially homogenous C3 un-rodded model was developed. A separate tally of just the flux was not undertaken; the flux is embedded in the fission reaction rate tally and is used instead. The fraction of a one percent change in the fission reaction rate of Figure 10 below is acceptable. A tilt does not exist in the results below, the flux solution has converged. The solution is well within one MCNP standard deviation.

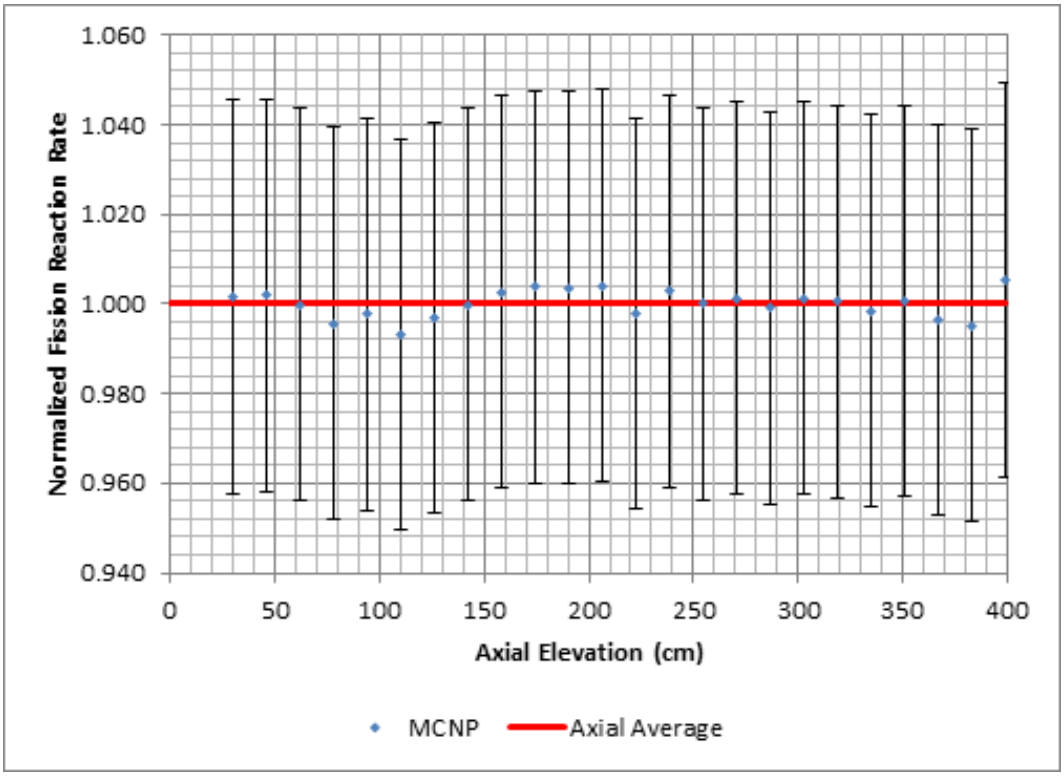

Figure 10: 3D C3 ARO MCNP Axially Homogeneous Core Flux Convergence

After the convergence of the reference MCNP results was demonstrated ITDM was run for the 3D C3 ARO test case and the comparisons between the two sets of predictions are shown in Table 8.

Table 8: 3D C3 ARO ITDM to MCNP Assembly Differences

k_{eff}	Reference (2 pcm)	1.22348	
	ITDM	1.22321	
	Difference (pcm)	-27	
Fission Reaction Rate Distribution	Reference	1.1917	0.8097
	ITDM	1.1904	0.8096
	Abs. % Difference	-0.13	-0.01
	Reference	0.8095	1.1891
	ITDM	0.8096	1.1904
	Abs. % Difference	-0.01	0.13

The eigenvalue and assembly relative fission reaction rate absolute percent differences are excellent; however there exists an axial tilt in the axial comparison between ITDM and MCNP as shown in Figure 11. The reasons for such tilt are being investigated by using continuous energy MCNP models to determine whether those are pointing out towards the flat flux approximation in PARAGON. The negative effects of such approximation have been minimized in radial plane by performing mesh-refining studies with PARAGON as described earlier in the paper. If the reason for axial tilt is determined to be the flat flux approximation in PARAGON we will search approaches to minimize its impact in axial direction.

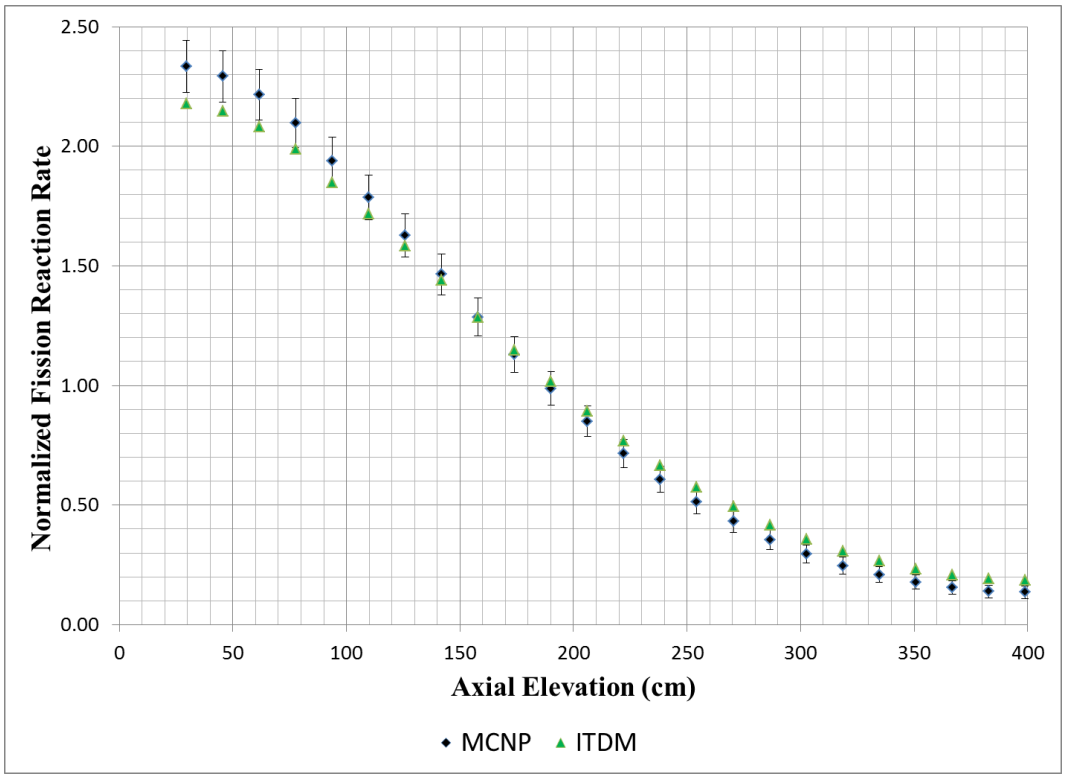

Figure 11: 3D C3 Core Fission Reaction Rate Shape

The non-linear iteration methodology utilized in ITDM can be optimized through additional PARAGON lattice calculations before the next NEM nodal solution as described earlier and reiterated here. In this scenario PARAGON is run an additional time and will utilize

the partial current boundary condition shape from the previous PARAGON calculation of the current iteration, and the node-wise surface-average incoming partial current from NEM. The transport solution from PARAGON will have an extra calculation by which it can converge. Initially the additional PARAGON calculations were started at later cycles, but it was found that the additional calculations are best when started in the second non-linear iteration. As the non-linear iterations continue, the shapes of the boundary conditions appear to converge because the relative pin fission reaction rates do not change within the lattice. Three PARAGON calculations per non-linear iteration were found to be optimal, future work should include determining if this is optimal for other core configurations and conditions not covered here.

3.4.6 Conclusion

The ITDM methodology provides very promising results when using partial currents as boundary conditions for loosely coupling a 2D lattice transport code to a 3D core nodal solver. The use of partial currents is a major improvement over albedos; the solutions converged in a smoother manner.

The future work includes resolving the axial tilt issue, and application of ITDM to test cases including reflectors. The 2D C3 model will be expanded to 2D C5 with radial reflector as previously shown in Figure 3.

This configuration will be analyzed also in ARO, Rodded-A and Rodded-B cases. The 2D C5 problem will be expanded to a 3D C5 problem by adding axial heterogeneities like moderator density and temperature axial distributions similar to the 3D C3 problem and axial reflectors. Based on this 3D C5 problem ARO and Rodded-A and Rodded-B cases will be analyzed to demonstrate the methodology for challenging realistic applications.

3.5 Overview of Thesis Contributions

First, the previous results of the project were reproduced in order to become familiarized with the programs and to verify that they were running correctly. Next, the moderator density values were updated from room temperature values to more realistic values that could be expected in a typical PWR. This task was a significant undertaking since this required a complete overhaul of the MCNP input. Once completed in MCNP, density values were also updated in ITDM for comparison.

The 3D inputs were broken down into individual two dimensional layers and run with MCNP and PARAGON for comparison. It was discovered that MCNP5 lacked the ability to accurately simulate the axial temperature distribution since the cross section libraries were only available for specific temperatures in increments of 300 Kelvin. Therefore, MCNP6 was installed and used to generate On the Fly (OTF) cross section libraries that accounted for the temperature changes. MCNP6 was also used to generate temperature interpolated cross section libraries that take into consideration the effects caused by the nature of the moderator being a chemical compound as opposed to the free gas treatment that was previously used. The MCNP inputs were then run in MCNP6 using these generated temperature sensitive cross sections to get the most accurate basis for comparison for ITDM.

The axial tilt seen in the previous results still remained. Therefore, the cause of the tilt has been the focus of the investigations in this thesis. In ITDM, various input parameters such as NEM mesh sizes, paragon radial discretization, the B1 approximation, and inter-layer axial leakage have been examined and compared to see the effects they have on the axial tilt and multiplication factor.

CHAPTER 4
INITIAL STATUS AND PRELIMINARY UPDATES

4.1 Initial Status and Reproduction of Previous Results

Previous work on ITDM has shown that the methodology works for full core simulations using burn-up steps. It has been found that using partial current boundary conditions has led to very promising results. Radially, the solutions have been found to be rather accurate, though issues are seen in in the axial reaction rate predictions. Reflector convergence issues have also been reported. (Colameco D. , 2012) This thesis focuses mainly on the investigation and correction of the axial tilt seen in the current results.

During the process of learning the programs and operating system used for the project, the results obtained in Dr. Colameco's dissertation were reproduced. The C3 ARO reference results were reproduced using the 70 group PARAGON generated cross section library in MCNP5. The 70 group MCNP library was generated in order to mitigate differences between the reference simulation and the ITDM prediction that could be caused by differences in the cross sections being used. This library was created using PARAGON generated cross sections in NJOY for each specific region of the simulation. NJOY assigned these specific values to MCNP material numbers used in the MCNP input files. Each region in the simulation had its own specific material number that corresponded to its PARAGON generated cross section set. Therefore, over 1000 MCNP input files were required because MCNP can only tally over 99 different material numbers in a single input file and thousands of material numbers existed for the simulation. The custom cross section libraries can be found in File 34 listed in Table 29 in Appendix A; a sample MCNP input file can be found in File 8. The ITDM source was then installed and a C3 ARO input from Dr. Colameco's work was run. The input file used can be

found in File 1. Upon comparison to Dr. Colameco's thesis, it was seen that the results for both ITDM and MCNP were successfully reproduced. (Colameco D. , 2012) The axial fission reaction rate distributions are shown in Figure 12, Figure 13, and Figure 14. The multiplication factor results are shown in Table 9. Only one of each of the UOX and MOX assemblies is shown, since the core is symmetric and results are mirrored.

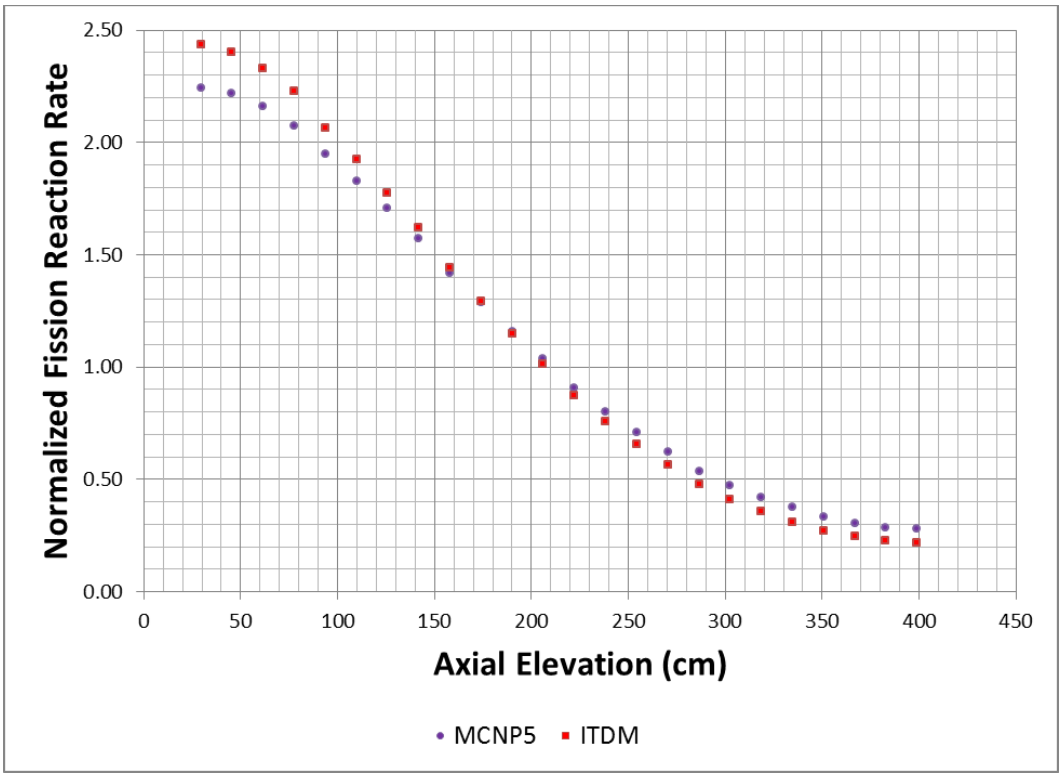

Figure 12: C3 ARO NW UOX Assembly Reproduction of Results

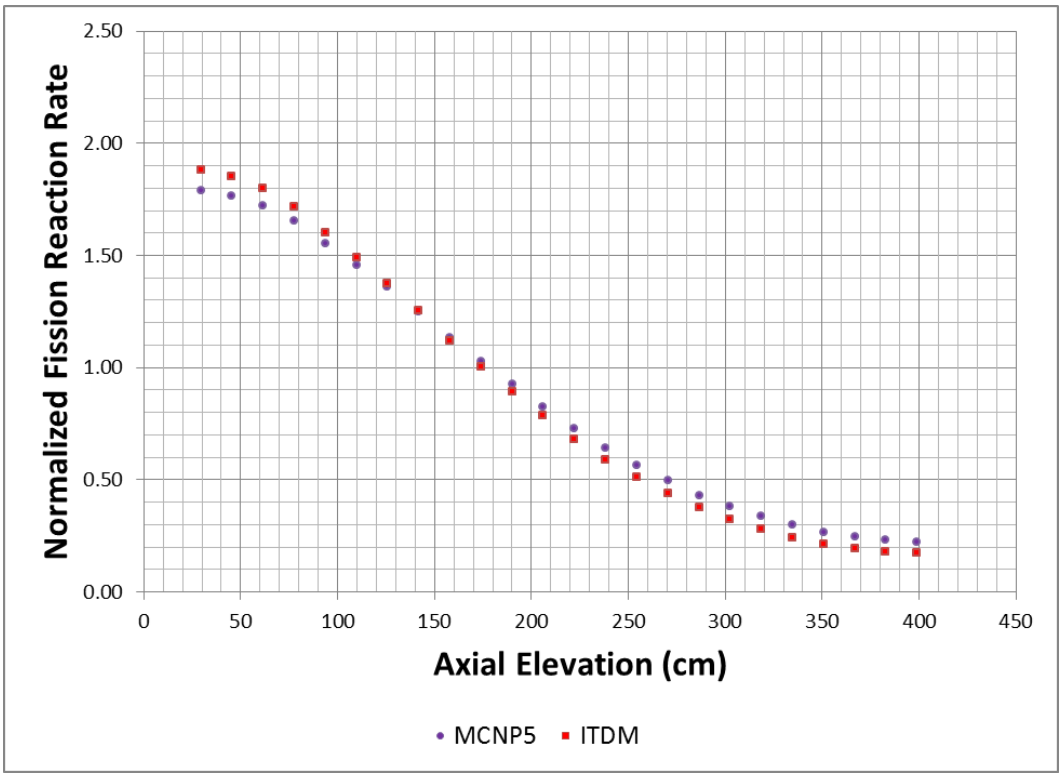

Figure 13: C3 ARO NE MOX Assembly Reproduction of Results

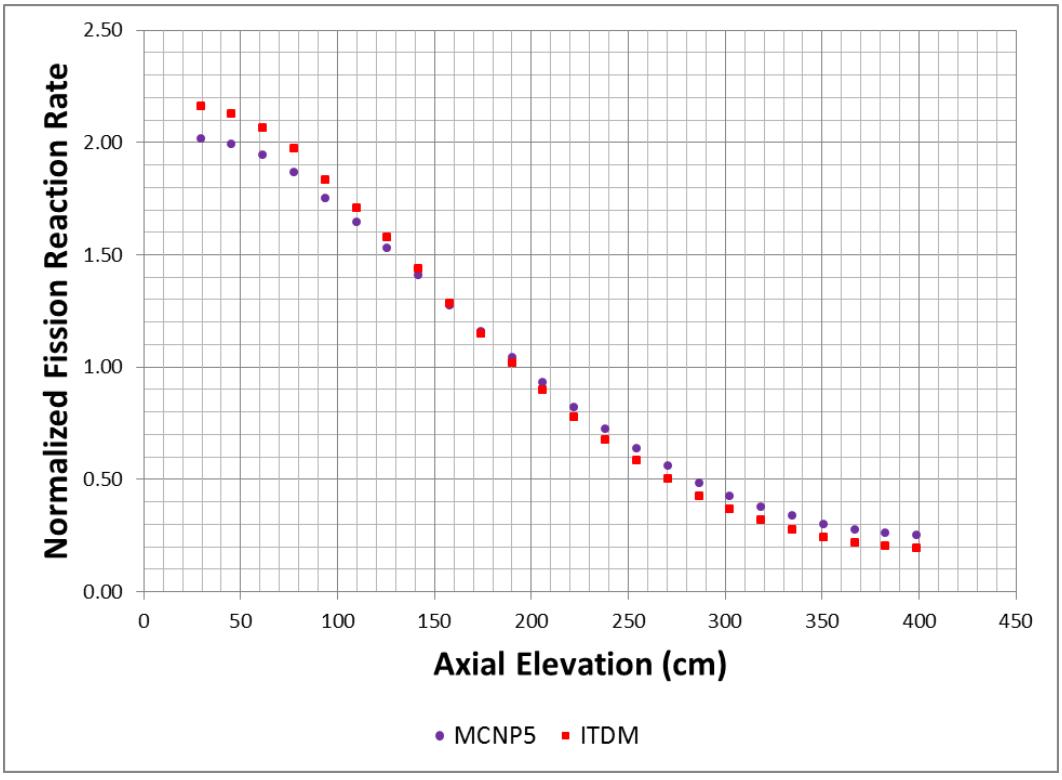

Figure 14: C3 ARO Core Average Reproduction of Results

Table 9: C3 ARO Core Average Multiplication Factor Reproduction of Results

	K_{eff}	Difference (pcm)
MCNP5	1.22574	-
ITDM	1.22462	112

It can be seen above that the axial fission reaction rate distribution is not correctly predicted by the ITDM code. The ITDM code biases the reaction rate more toward the bottom of the core, creating a "tilt" in the distribution. However, it is important to note that the moderator properties for each of these simulations are based on room temperature. It is possible that some the assumptions in the ITDM code, specifically the flat-flux approximation used in PARAGON, may be invalid for these properties. Therefore, the moderator properties require updating before further testing is to be done.

4.2 Moderator Density Update

After reproducing the results from Dr. Colameco's dissertation, the moderator properties were updated. This change was implemented because the custom libraries explained above were generated using room temperature properties for the moderator. It was decided that the 70 group MCNP library method explained in the previous section would not be reused because of the complications and extremely long run times that it presented. Therefore, new MCNP inputs were written to simulate the same core using the standard ENDF/B6 continuous energy libraries included with MCNP5. This allowed the material properties and compositions to be programmed into the MCNP inputs, rather than the cross section libraries. However, this removed the moderator temperature variation in the axial direction. In MCNP5 the moderator temperature was fixed at 600 Kelvin for the entire core. The moderator densities, however, were still able to be varied axially to reflect the simulation at hot full power. These changes decrease the number of MCNP input files for a single core to 4, rather than thousands, since an entire assembly could be tallied in a single file. Statistics were retained since the number of histories run per file remained unchanged.

Another benefit that was realized from having such a low number of files is that parallelization could now be used. Extremely similar results were obtained using the new inputs (with the non-updated densities) for verification.

Table 10 below outlines the temperatures and densities used in each layer of the simulation to this point. The "Non-updated" section refers to the room temperature densities that were used in the previous work for both MCNP and ITDM. The ITDM-Updated section refers to the densities and temperatures that best reflect the conditions that are being simulated. The

MCNP-Updated section refers to the same densities, only with the temperatures being held constant due to the restrictions of MCNP5. It can be seen that the difference in density is quite significant.

Table 10: Moderator Properties by Layer with MCNP5 Temperatures

Layer1	**Moderator Temp [K]**	**Moderator Density [g/cm^3]**	**Hydrogen #Density [1/(b-cm)]**	**Oxygen #Density [1/(b-cm)]**	**Boron #Density [1/(b-cm)]**
ITDM-Updated	561.75	0.736568	4.9252E-02	2.4626E-02	4.0798E-06
MCNP-Updated	600.00	0.736568	4.9252E-02	2.4626E-02	4.0798E-06
Non-updated	561.75	1.003945	6.7118E-02	3.3559E-02	5.5252E-06
Layer 2	**Moderator Temp [K]**	**Moderator Density [g/cm^3]**	**Hydrogen #Density [1/(b-cm)]**	**Oxygen #Density [1/(b-cm)]**	**Boron #Density [1/(b-cm)]**
ITDM-Updated	569.05	0.7275696	4.8651E-02	2.4325E-02	4.0299E-06
MCNP-Updated	600.00	0.7275696	4.8651E-02	2.4325E-02	4.0299E-06
Non-updated	569.05	0.9917204	6.6301E-02	3.3151E-02	5.4580E-06
Layer 3	**Moderator Temp [K]**	**Moderator Density [g/cm^3]**	**Hydrogen #Density [1/(b-cm)]**	**Oxygen #Density [1/(b-cm)]**	**Boron #Density [1/(b-cm)]**
ITDM-Updated	575.80	0.7192710	4.8096E-02	2.4048E-02	3.9840E-06
MCNP-Updated	600.00	0.7192710	4.8096E-02	2.4048E-02	3.9840E-06
Non-updated	575.80	0.9803690	6.5542E-02	3.2771E-02	5.3955E-06
Layer 4	**Moderator Temp [K]**	**Moderator Density [g/cm^3]**	**Hydrogen #Density [1/(b-cm)]**	**Oxygen #Density [1/(b-cm)]**	**Boron #Density [1/(b-cm)]**
ITDM-Updated	583.00	0.7104726	4.7507E-02	2.3754E-02	3.9352E-06
MCNP-Updated	600.00	0.7104726	4.7507E-02	2.3754E-02	3.9352E-06
Non-updated	583.00	0.9683627	6.4740E-02	3.2370E-02	5.3294E-06
Layer 5	**Moderator Temp [K]**	**Moderator Density [g/cm^3]**	**Hydrogen #Density [1/(b-cm)]**	**Oxygen #Density [1/(b-cm)]**	**Boron #Density [1/(b-cm)]**
ITDM-Updated	590.95	0.7008743	4.6866E-02	2.3433E-02	3.8821E-06
MCNP-Updated	600.00	0.7008743	4.6866E-02	2.3433E-02	3.8821E-06
Non-updated	590.95	0.9552649	6.3864E-02	3.1932E-02	5.2573E-06
Layer 6	**Moderator Temp [K]**	**Moderator Density [g/cm^3]**	**Hydrogen #Density [1/(b-cm)]**	**Oxygen #Density [1/(b-cm)]**	**Boron #Density [1/(b-cm)]**
ITDM-Updated	598.25	0.6918759	4.6264E-02	2.3132E-02	3.8322E-06
MCNP-Updated	600.00	0.6918759	4.6264E-02	2.3132E-02	3.8322E-06
Non-updated	598.25	0.9430403	6.3047E-02	3.1523E-02	5.1901E-06

The results obtained with the updated moderator compositions outlined above are shown in Figure 15, Figure 16, and Figure 17 below. These results are tabulated in File 17 listed in Table 29.

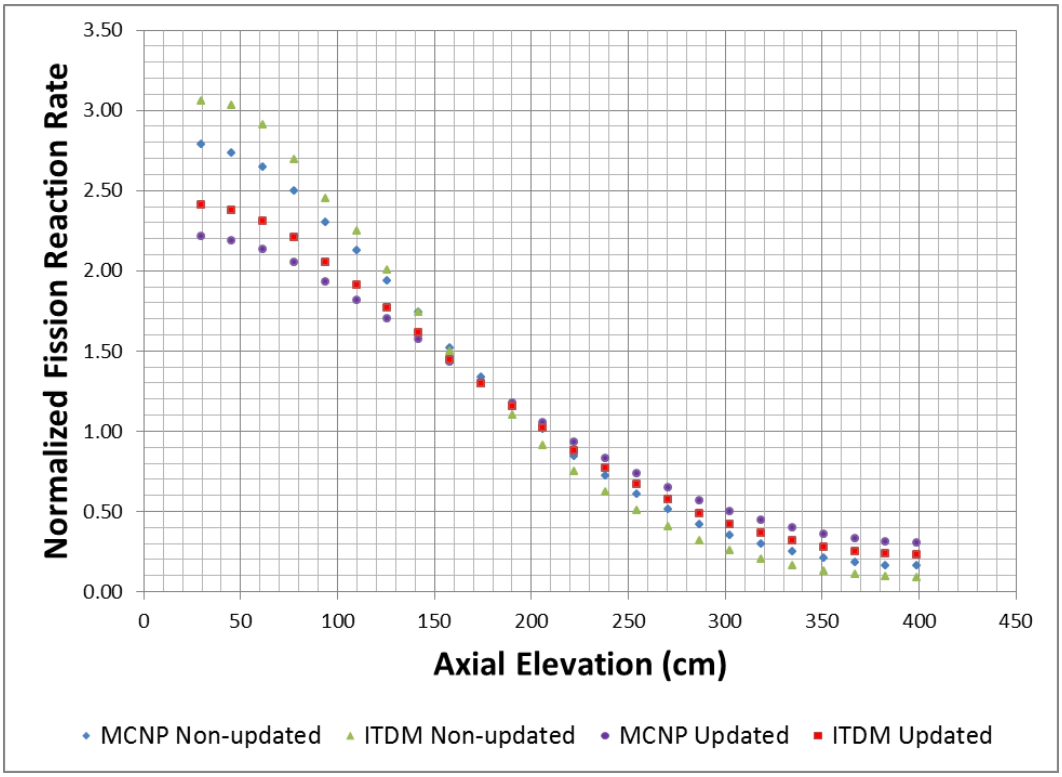

Figure 15: C3 ARO NW UOX Assembly Density Update Comparison

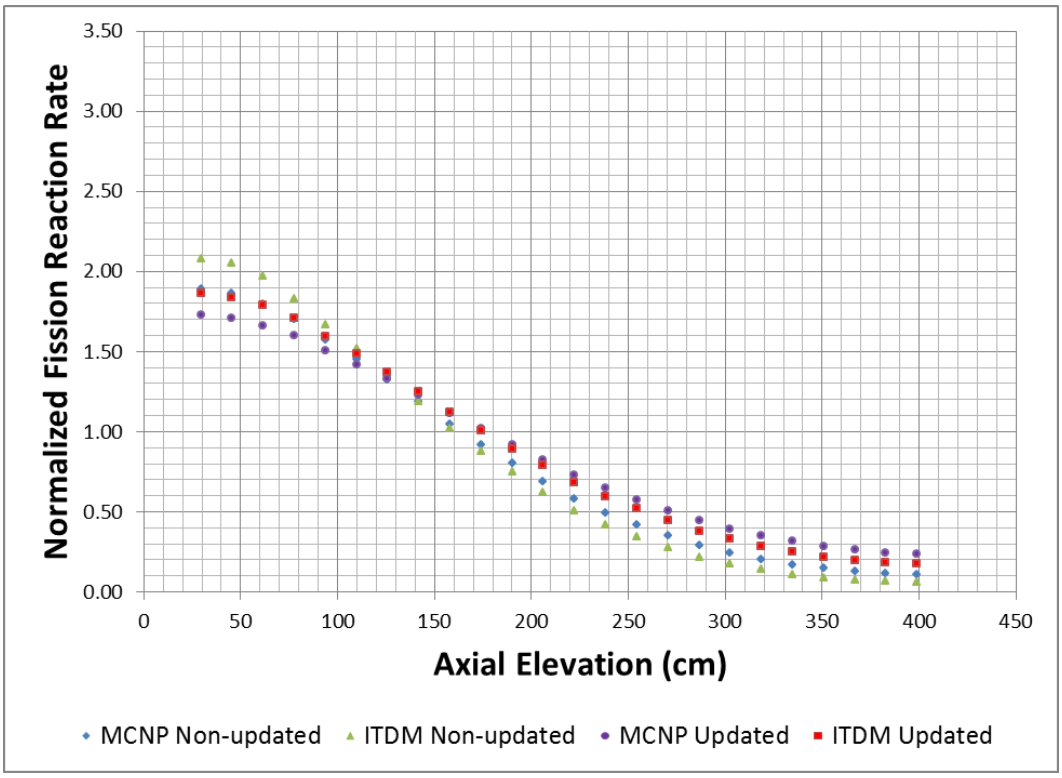

Figure 16: C3 ARO NE MOX Assembly Density Update Comparison

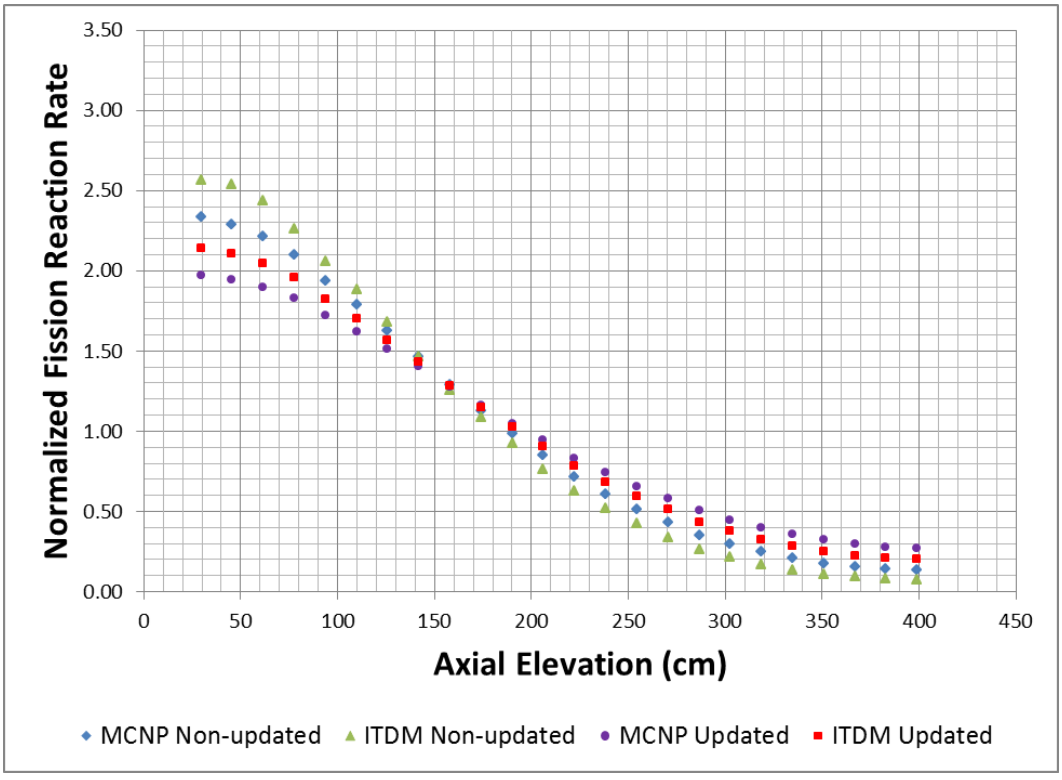

Figure 17: C3 ARO Core Average Density Update Comparison

It can be seen above that the updated density has a significant impact on the axial fission reaction rate distribution, as is expected. Less variation is seen along the length of the core. However, it is clear that the axial tilt has not been remedied.

Table 11 shows the multiplication factors received from the simulations with the updated density values. The non-updated values are also included for comparison. It can be seen that the difference in multiplication factors between ITDM and MCNP has been significantly increased. It was hypothesized that this difference is due to the temperature differences being modeled due to the restrictions of MCNP5.

Table 11: C3 ARO Core K_{eff} Density Update Comparison

ITDM Updated	MCNP Updated	Difference (pcm)
1.1721	1.18627	1417
ITDM Non-updated	**MCNP Non-updated**	**Difference (pcm)**
1.22462	1.22574	112

4.3 MCNP6 Temperature Update

Since the multiplication factor difference increased significantly in the results from the previous section, it was decided that the temperature changes in the axial direction needed to be modelled more correctly in MCNP. Therefore, MCNP5 was replaced with MCNP6 and specific temperature designations were added to the cells in the input files. The "FIT_OTF" utility of MCNP6 was used to generate cross section libraries that were Doppler broadened for the desired temperatures for each of the materials in the core. (Martin, Wilderman, Brown, & Yesilyurt, 2013) These cross section libraries can be found in File 33 listed in Table 29.

It was discovered that the MCNP5 results above treated the moderator as a free gas, rather than a chemical compound. MCNP6 was used to broaden the "lwtr" cross section libraries for the desired temperatures in order to account for the nature of the chemical compound at the desired temperatures. The broadened library and its directory can be found in File 34 listed in Table 29. It is important to note that the main MCNP cross section directory file was appended to include the newly generated directory and the library which contained the new broadened cross sections.

MCNP6 was then run with the temperature changes described above. Figure 18, Figure 19, and Figure 20 below show the MCNP6 results compared to the MCNP5 and ITDM updated results from the previous section. These results are tabulated in File 16 listed in Table 29.

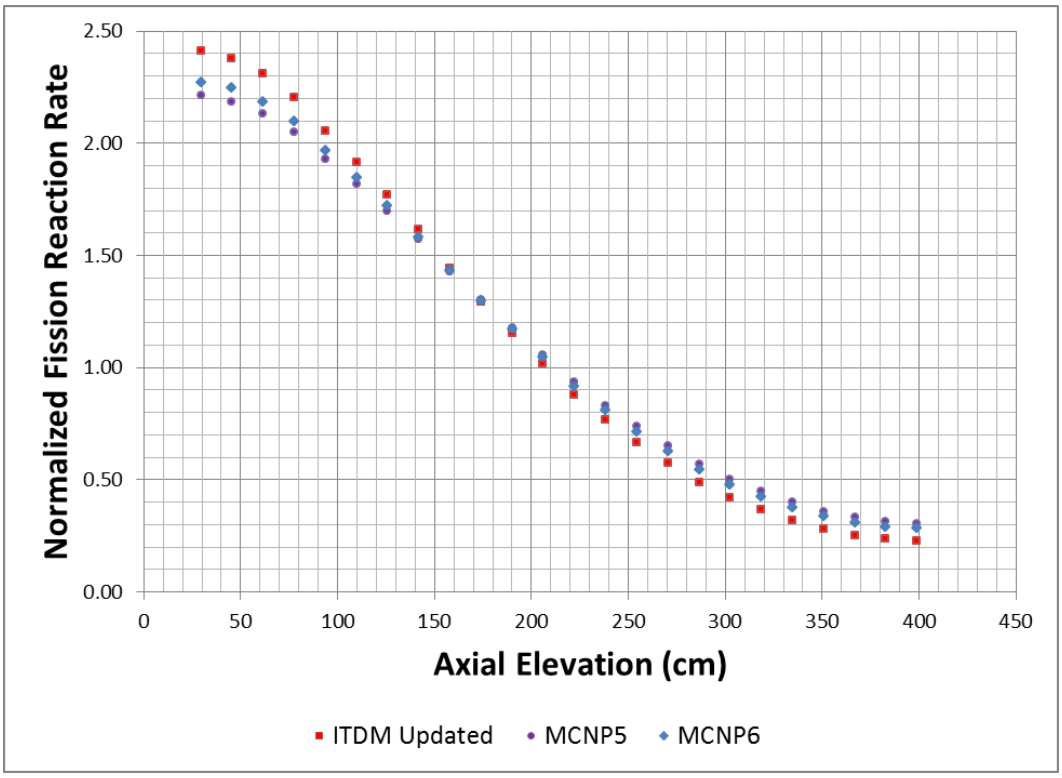

Figure 18: C3 ARO NW UOX Assembly Temperature Update Comparison

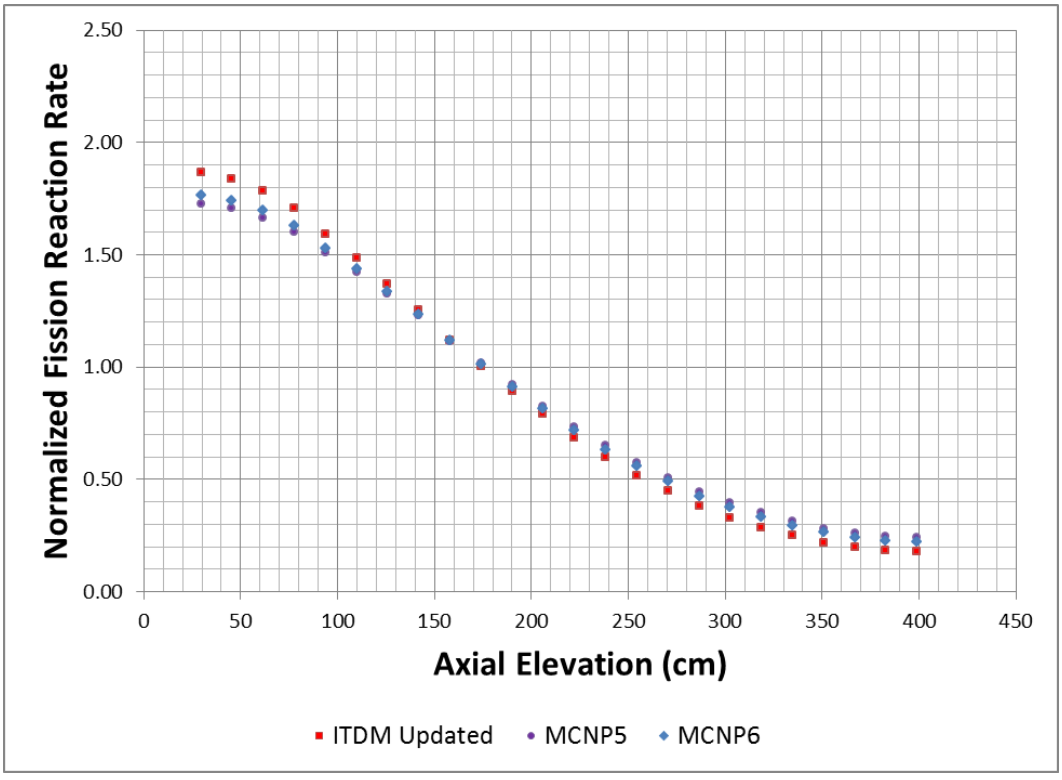

Figure 19: C3 ARO NE MOX Assembly Temperature Update Comparison

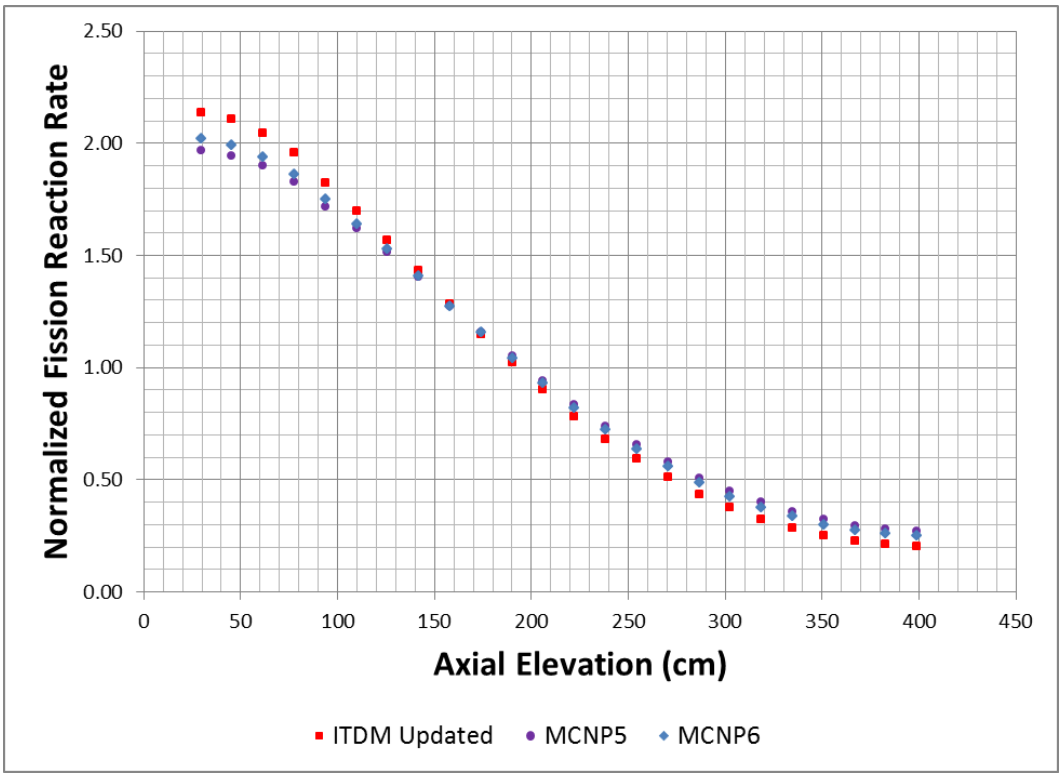

Figure 20: C3 ARO Core Average Temperature Update Comparison

It can be seen that MCNP6 with the appropriate temperature update yielded a solution slightly closer to that of the updated ITDM run with respect to the axial reaction rate distribution. In Table 12 below, it can be seen that the multiplication factor is now much more consistent with the ITDM results. It was decided that the MCNP6 run would serve as a basis of comparison for the remaining work in ITDM.

Table 12: C3 ARO Core K_{eff} Temperature Update Comparison

	K_{eff}	Difference (pcm)
ITDM Updated	1.1721	-
MCNP5	1.18627	1417
MCNP6	1.17367	157

CHAPTER 5
AXIAL POWER TILT STUDIES

5.1 NEM Discretization Study

After establishing the MCNP6 basis using the updated temperatures and densities, ITDM options were explored to determine their effects on the results. First, the axial and radial meshes in NEM were refined. Axially, ITDM was run with 24, 48, and 96 layers for comparison. The results of this comparison can be seen below in Figure 21, Figure 22, and Figure 23. It can be seen that the axial reaction rate distributions were nearly identical for each case. Minimal improvement was seen in the axial reaction rate distributions by refining the axial mesh. The full results can be seen in File 18 listed in Table 29.

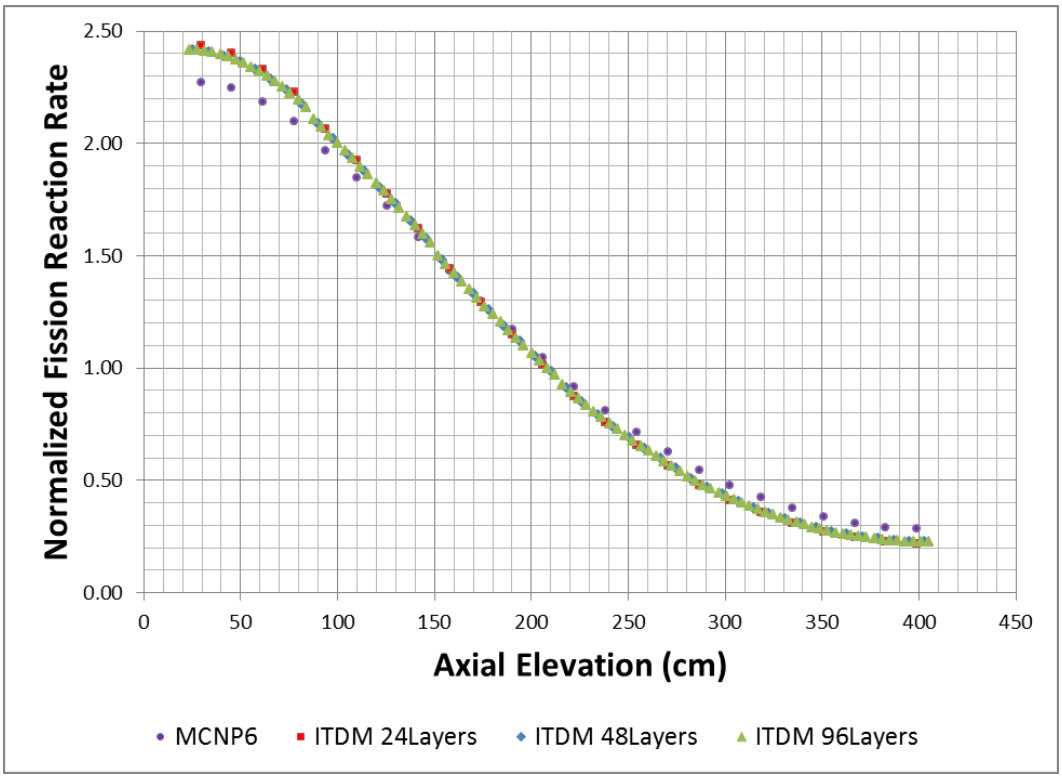

Figure 21: C3 ARO NW UOX Assembly NEM Axial Mesh Comparison

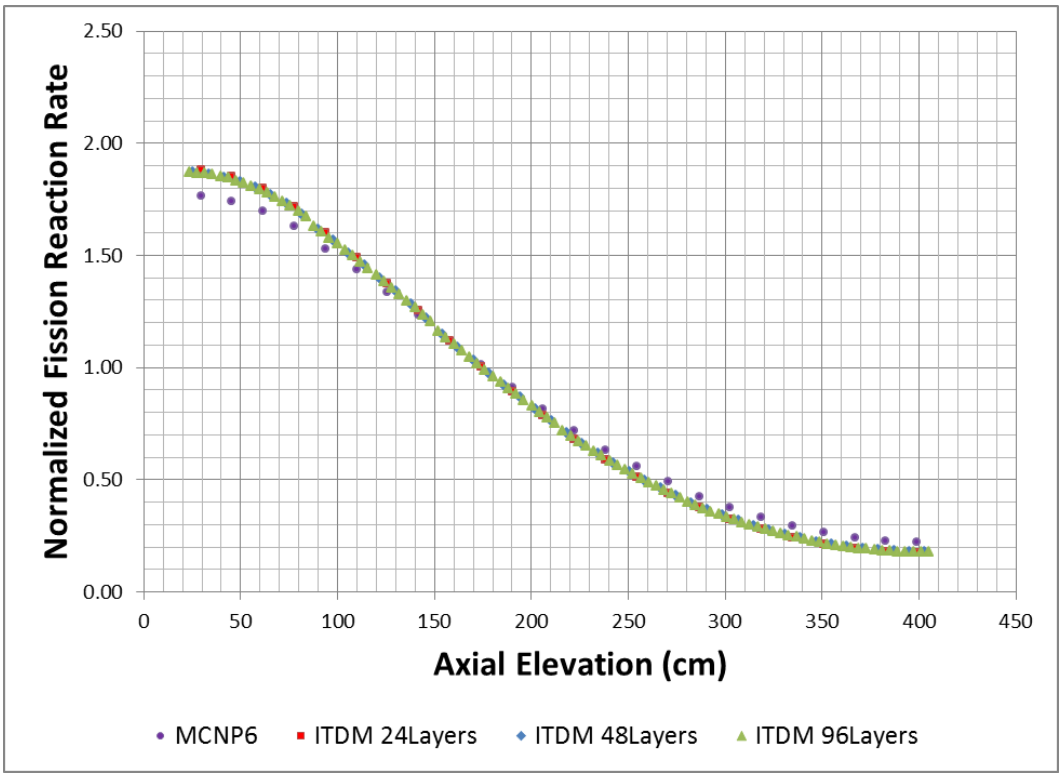

Figure 22: C3 ARO NE MOX Assembly NEM Axial Mesh Comparison

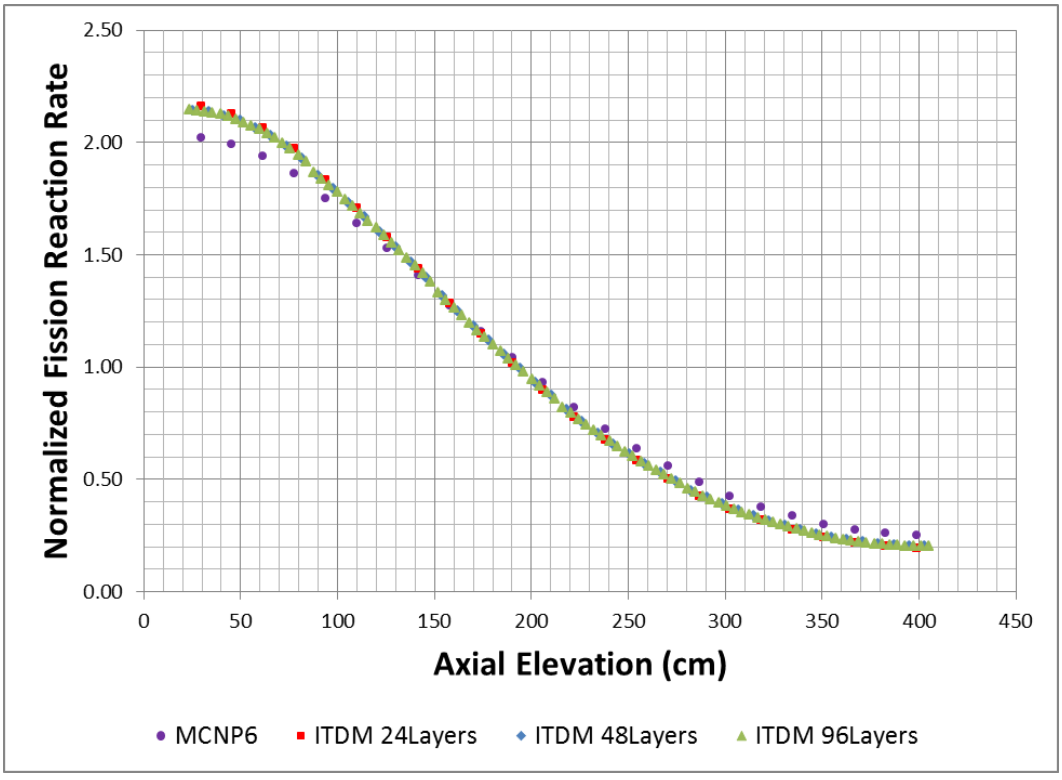

Figure 23: C3 ARO Core Average NEM Axial Mesh Comparison

Next, the radial meshing in NEM was examined. Two cases were run: 1 radial node per assembly (1NPA) and 289 radial nodes per assembly (pin-by-pin or PxP). In each of these cases, 24 axial layers were used. The results can be seen below in Figure 24, Figure 25, and Figure 26. Once again, the axial reaction rate distributions between cases were nearly identical, with the 1NPA case showing minimally better agreement. Full results are included with the axial mesh comparison results.

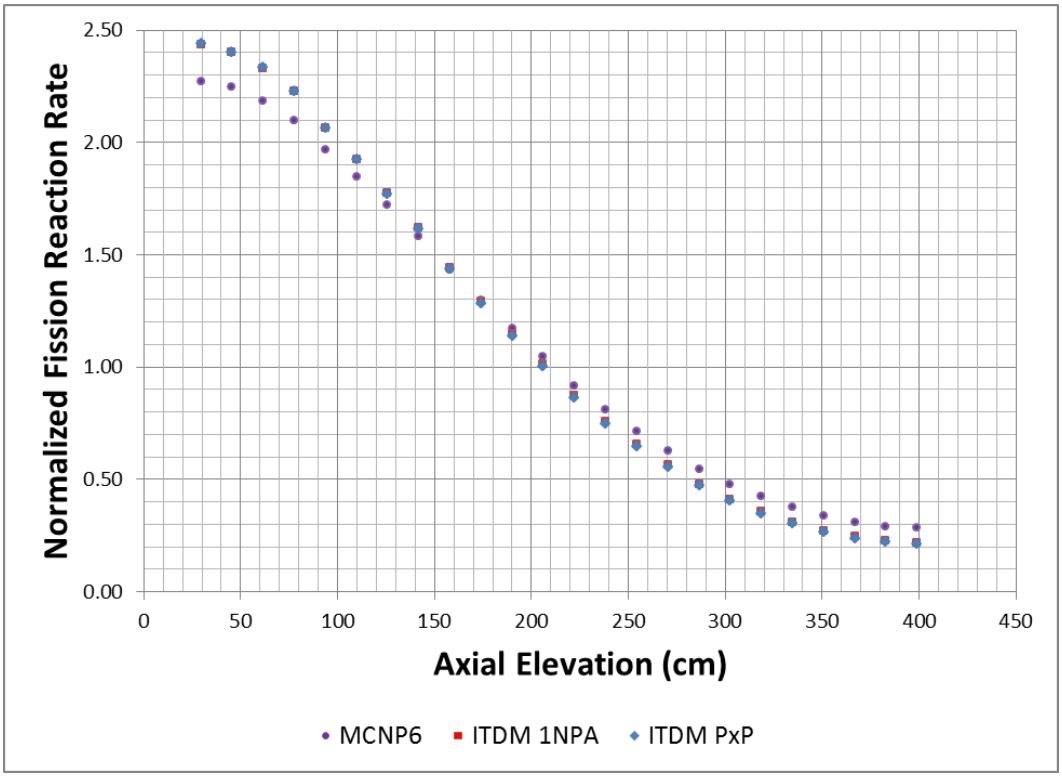

Figure 24: C3 ARO NW UOX Assembly NEM Radial Mesh Comparison

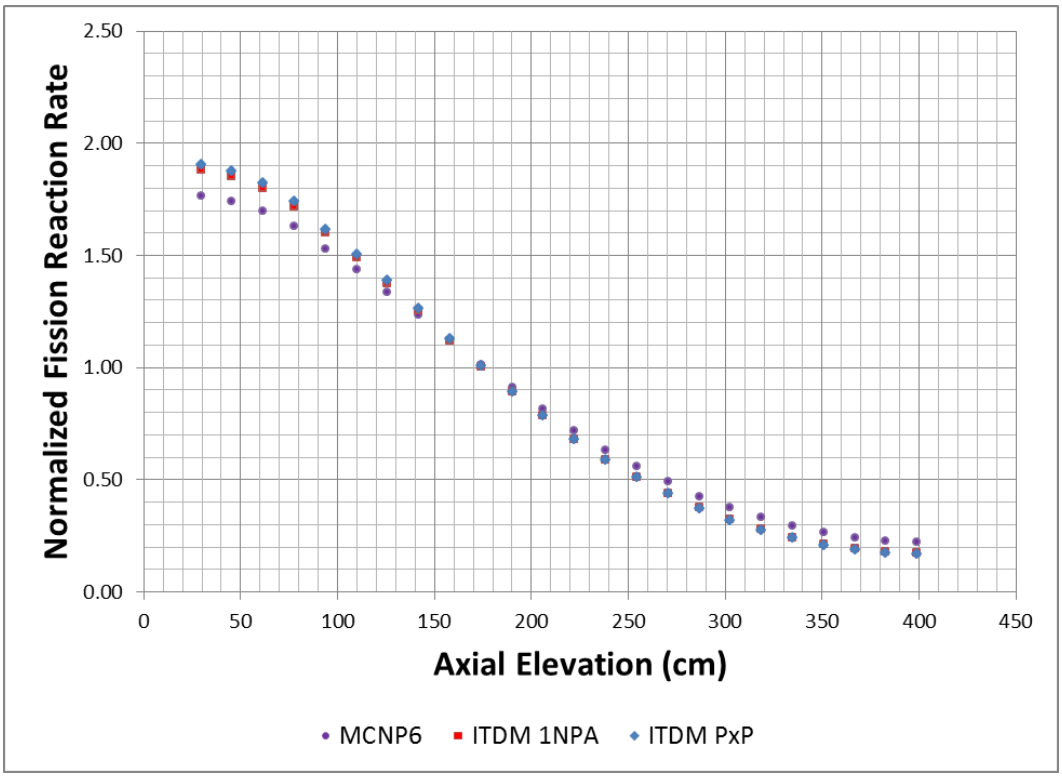

Figure 25: C3 ARO NE MOX Assembly NEM Radial Mesh Comparison

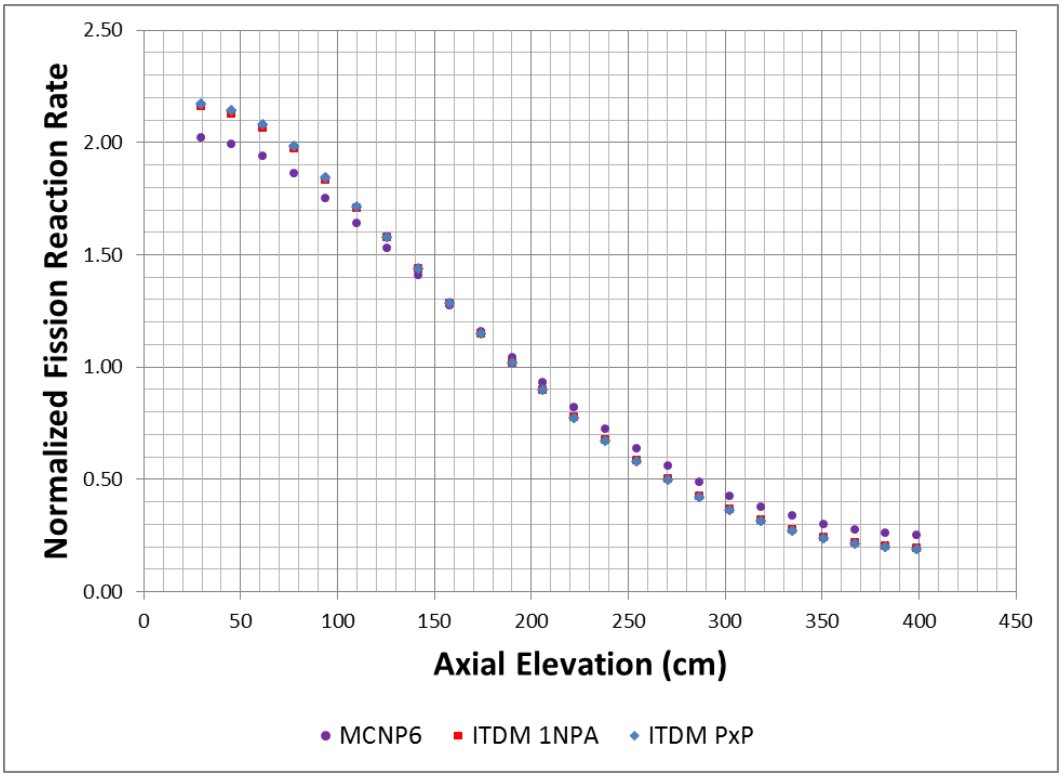

Figure 26: C3 ARO Core Average NEM Radial Mesh Comparison

The multiplication factors for each of the above runs have been tabulated in

Table 13 below. It can be seen that decreasing the mesh size in either direction actually has a detrimental effect to the accuracy of the multiplication factor. The most accurate case remains the 1NPA 24 layer case.

Table 13: C3 ARO Core K_{eff} NEM Discretization Comparison

	K_{eff}	Difference (pcm)
MCNP	1.17367	-
ITDM PxP 24 Layers	1.16813	554
ITDM 1NPA 24 Layers	1.17226	141
ITDM 1NPA 48 Layers	1.17209	158
ITDM 1NPA 96 Layers	1.17209	158

The individual pin power errors are shown below. These Pin Power comparisons are made in File 19 listed in Table 29. Table 14 shows the absolute percent difference errors for the 1NPA calculation. Table 15 shows the same errors for the pin-by-pin case. It can be seen that the errors between the two cases are similar, with the 1NPA case having slightly lower errors. The maximum and minimum errors are seen in the MOX assemblies, near the bottom of the core for both cases. The averaged errors in these tables were calculated using absolute values to ensure that positive and negative errors did not cancel out in the average.

Table 14: C3 ARO Pin Power Errors MCNP6 vs. ITDM 1NPA

Abs. % Diff	NW UOX	SE UOX	NE MOX	SW MOX
Core Max	21.50%	21.92%	16.12%	15.70%
Core Min	-8.62%	-8.73%	-6.87%	-6.84%
Core Avg	7.03%	7.02%	5.24%	5.25%
Max Layer RMS	16.63%	16.56%	11.64%	11.56%
Min Layer RMS	0.77%	0.93%	0.91%	0.97%
Avg Layer RMS	7.16%	7.15%	5.34%	5.35%

Table 15: C3 ARO Pin Power Errors MCNP6 vs. ITDM PxP

Abs. % Diff	NW UOX	SE UOX	NE MOX	SW MOX
Core Max	21.48%	22.00%	19.08%	18.35%
Core Min	-9.13%	-9.18%	-7.86%	-7.45%
Core Avg	7.47%	7.47%	6.00%	6.02%
Max Layer RMS	17.01%	16.93%	14.21%	14.13%
Min Layer RMS	1.18%	1.11%	1.01%	0.96%
Avg Layer RMS	7.65%	7.63%	6.12%	6.13%

It was found that the spatial discretization in NEM has little effect on the axial and radial power distributions. However, a more significant impact was seen in the multiplication factor prediction. This shows that refining the mesh in NEM, alone, is not beneficial to the simulation. Though, it should be noted that refining the mesh while applying other changes as well could lead to great improvements in the simulation.

5.2 PARAGON Discretization Study

Three levels of discretization were then tested in PARAGON, leaving NEM at 1NPA and 24 layers. The first level, “No”, treated the fuel and moderator sections of each pin as single rings each in the radial direction. The next level, “Low”, added octants in the polar direction. Finally, the “High” level used two rings each radially and octants in the polar direction. These discretization levels are depicted in Figure 27 below. The first cycle PARAGON input files for each of these cases are in Files 28, 29 and 30 listed in Table 29.

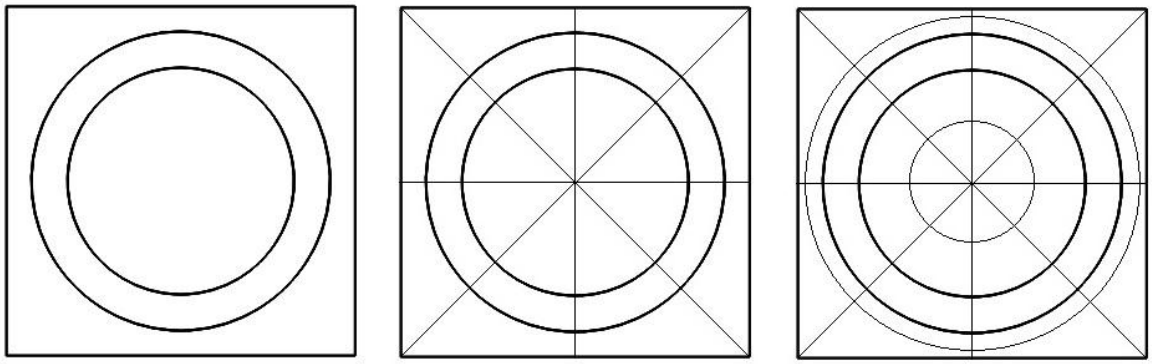

Figure 27: Paragon Radial Discretization Levels: No, Low, and High respectively

The results of these three runs are shown in Figure 28, Figure 29, and Figure 30 and are tabulated in File 20.

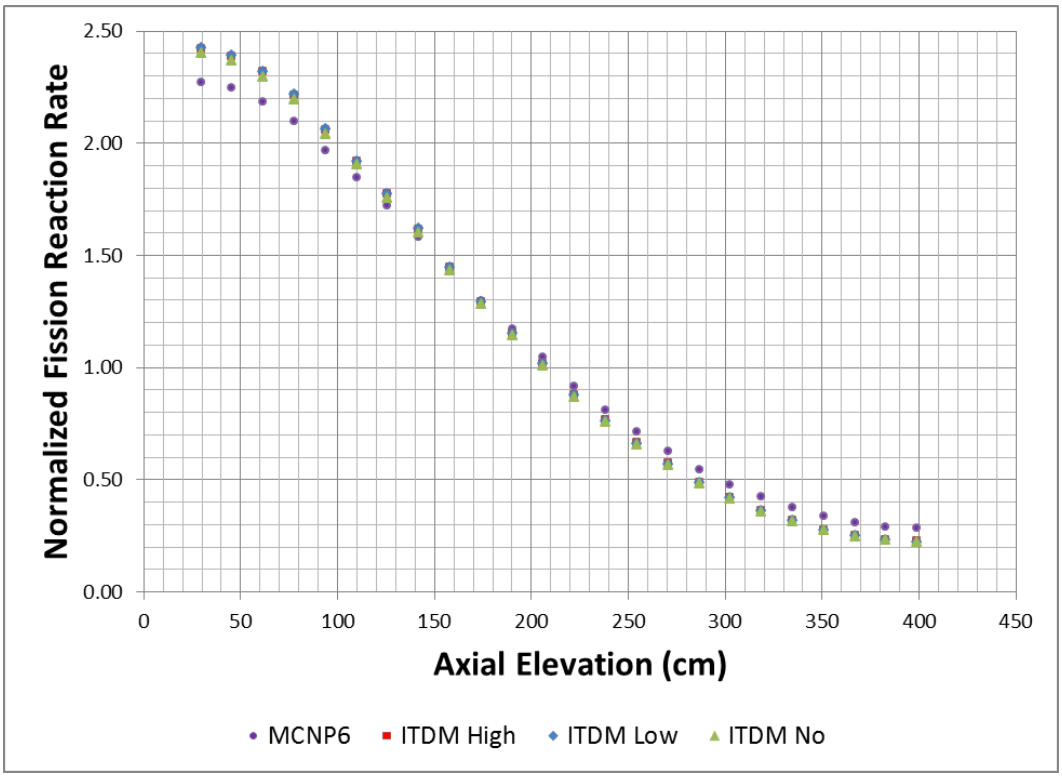

Figure 28: C3 ARO NW UOX Assembly PARAGON Discretization Comparison

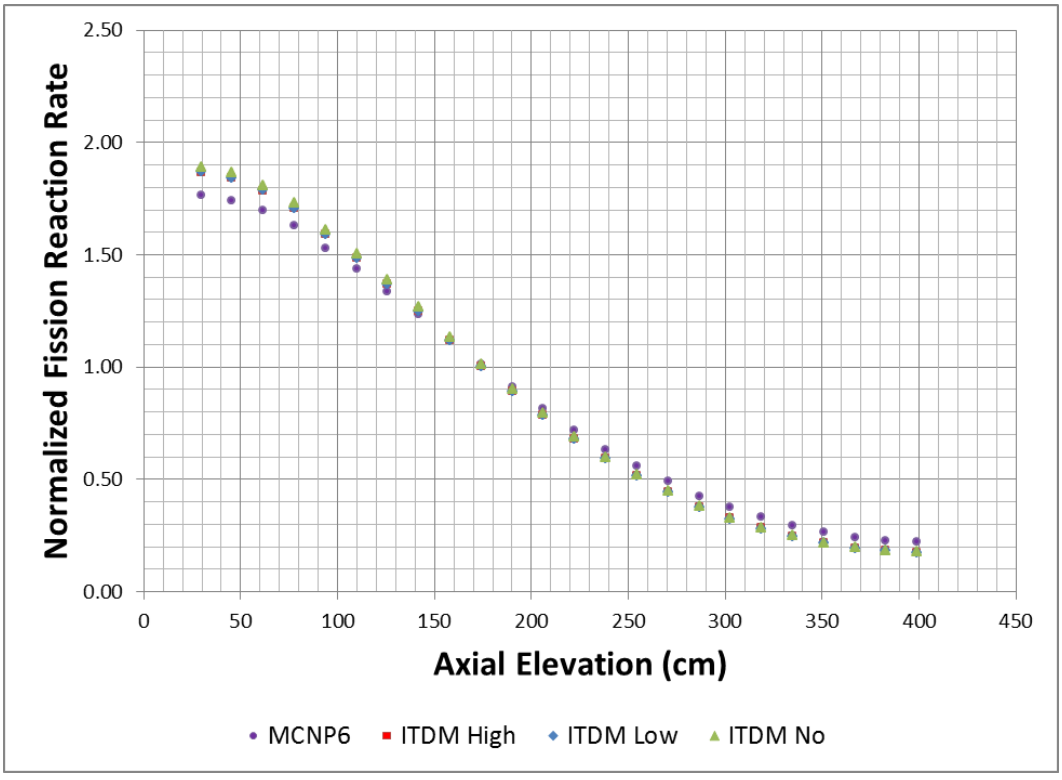

Figure 29: C3 ARO NE MOX Assembly PARAGON Discretization Comparison

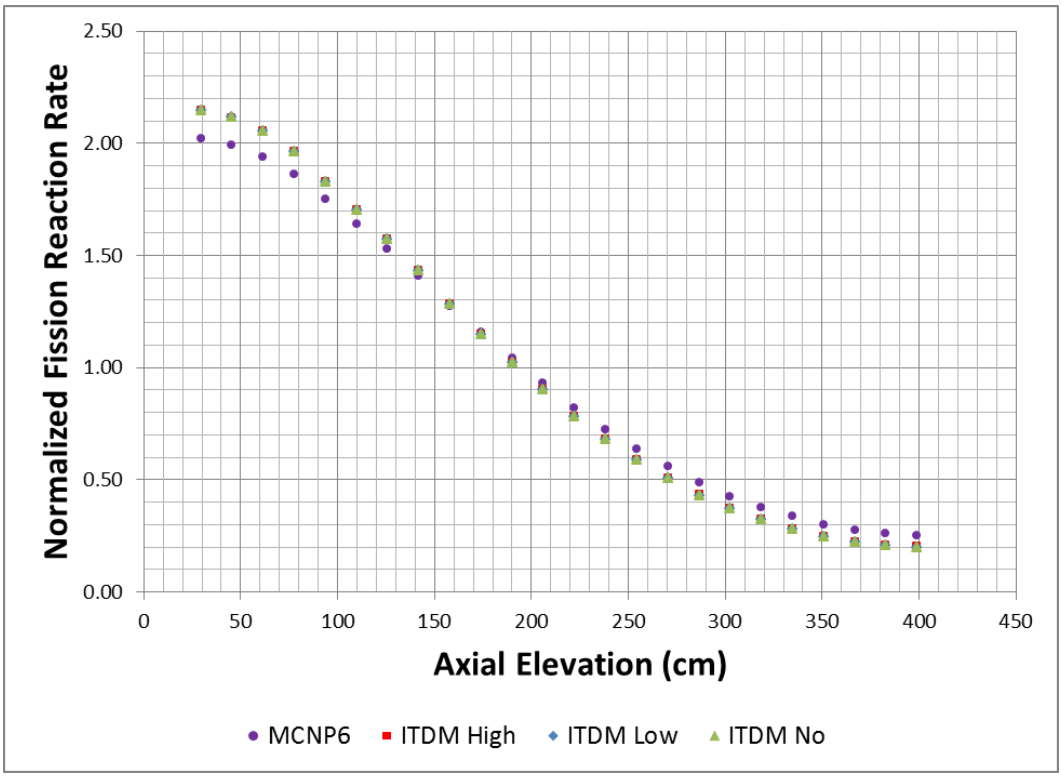

Figure 30: C3 ARO Core Average PARAGON Discretization Comparison

Again, the axial reaction rate distribution only has negligible changes throughout the core. However, Table 16 below shows that the discretization in PARAGON has a moderate effect on the multiplication factor. It can be seen that higher discretization produces more accurate results.

Table 16: C3 ARO Core K_{eff} PARAGON Discretization Comparison

	K_{eff}	Difference (pcm)
MCNP6	1.17367	-
ITDM High	1.17260	107
ITDM Low	1.17228	139
ITDM No	1.17213	154

The individual pin power errors for each case are shown below and can be found in File 21 listed in Table 29. Table 17 shows the absolute percent difference pin errors between MCNP6 and ITDM with high PARAGON discretization. Table 18 shows these results for the low case

and Table 19 shows the non-discretized errors. Again, it can be seen that increasing the level of discretization in PARAGON yields slightly better results in most cases. However, in the UOX assemblies the error was lowest for the no discretization case. It is important to note that increasing the level of discretization in PARAGON significantly impacts run time. The high discretization run used 163.9 CPU hours, the low run used 28.4 CPU hours, and the no run used 5.9 CPU hours.

Table 17: C3 ARO Pin Power Errors MCNP6 vs. ITDM High

Abs. % Diff	NW UOX	SE UOX	NE MOX	SW MOX
Core Max	18.34%	18.15%	16.42%	16.09%
Core Min	-7.63%	-7.69%	-6.33%	-6.35%
Core Avg	6.35%	6.34%	4.77%	4.78%
Max Layer RMS	14.94%	14.87%	10.58%	10.50%
Min Layer RMS	0.53%	0.70%	1.16%	1.19%
Avg Layer RMS	6.43%	6.42%	4.94%	4.95%

Table 18: C3 ARO Pin Power Errors MCNP6 vs. ITDM Low

Abs. % Diff	NW UOX	SE UOX	NE MOX	SW MOX
Core Max	18.72%	18.58%	16.79%	16.41%
Core Min	-7.79%	-7.81%	-6.44%	-6.47%
Core Avg	6.48%	6.47%	4.87%	4.88%
Max Layer RMS	15.26%	15.19%	10.81%	10.73%
Min Layer RMS	0.54%	0.70%	1.18%	1.20%
Avg Layer RMS	6.56%	6.55%	5.04%	5.05%

Table 19: C3 ARO Pin Power Errors MCNP6 vs. ITDM No

Abs. % Diff	NW UOX	SE UOX	NE MOX	SW MOX
Core Max	16.10%	15.75%	21.38%	20.48%
Core Min	-8.22%	-8.38%	-6.08%	-5.92%
Core Avg	6.09%	6.10%	5.25%	5.27%
Max Layer RMS	12.87%	12.79%	13.18%	13.10%
Min Layer RMS	0.72%	0.79%	1.25%	1.23%
Avg Layer RMS	6.20%	6.20%	5.46%	5.47%

The results of the discretization study in PARAGON show us that improvements to the multiplication factor and pin power errors can be had, but require significant processing time. It has also shown that the discretization in PARAGON is not the root of the tilt seen in the axial fission reaction rate distribution.

5.3 B1 Approximation Study

To this point, ITDM had been running without using the B1 approximation. The B1 approximation is used to adjust the critical neutron spectrum in the simulation. It uses a buckling search to adjust for the fact that the K_{eff} is significantly different than 1 because only a portion of a real core is being simulated. This is accomplished in PARAGON by performing a buckling search in which PARAGON obtains a criticality spectrum that is later used to collapse and homogenize the cross-sections. In ITDM, where the actual radial core environment is taken into account by the boundary conditions, this effectively helps account for the axial transference of neutrons in the core on the assembly level.

The C3 ARO hot full power (HFP) core was simulated using three options for the B1 approximation: off, on, and opt2. The off and opt2 options are the same except for the way in which the diffusion coefficient is calculated. “Off” calculates the diffusion coefficient using the standard diffusion approximation: the inverse of the product of 3 times the macroscopic transport cross section. This transport cross section is generated in PARAGON and is homogenized over each assembly and collapsed to the NEM macro group structure. Opt2 uses an asymptotic diffusion coefficient generated in the PARAGON output. This asymptotic diffusion coefficient is outlined in Dr. Colameco’s thesis. (Colameco D. , 2012)

The results of these runs can be seen below in Figure 31, Figure 32, and Figure 33 and can be found in File 14 listed in Table 29.

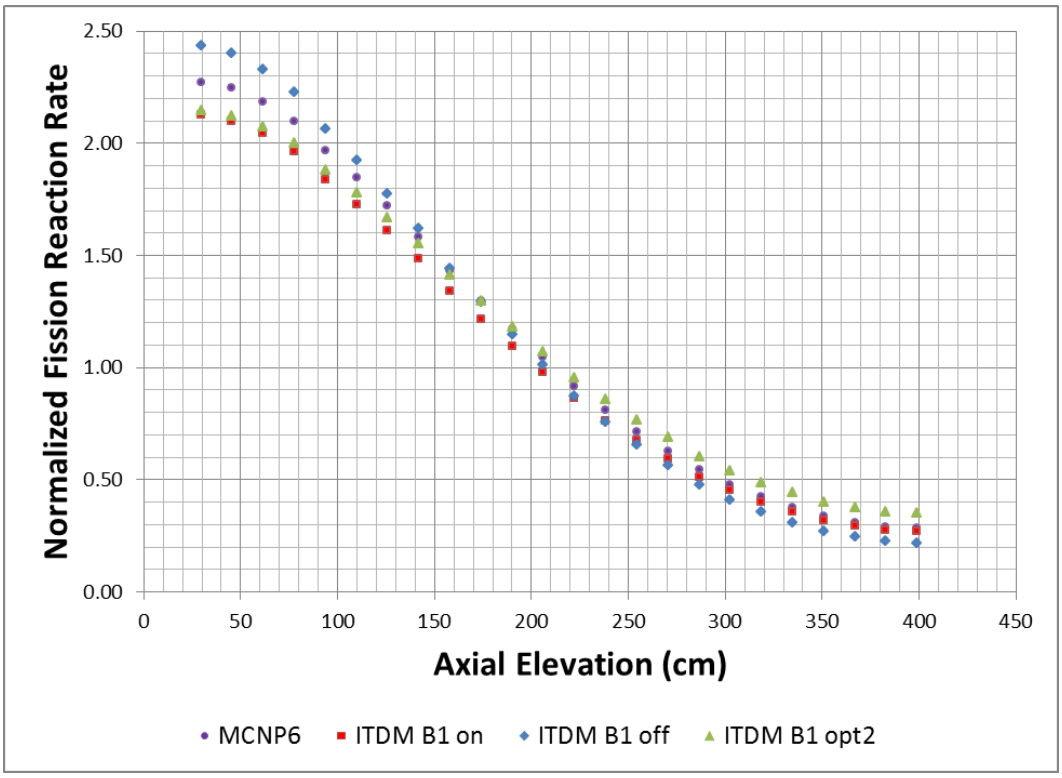

Figure 31: C3 ARO NW UOX Assembly B1 Comparison

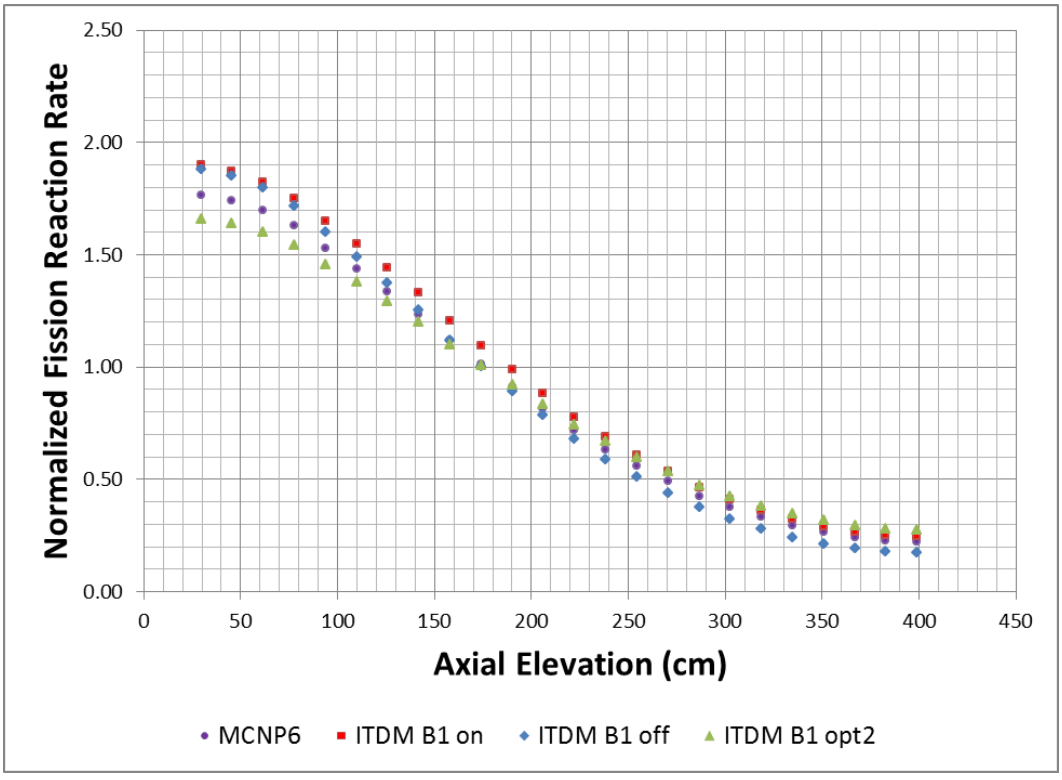

Figure 32: C3 ARO NE MOX Assembly B1 Comparison

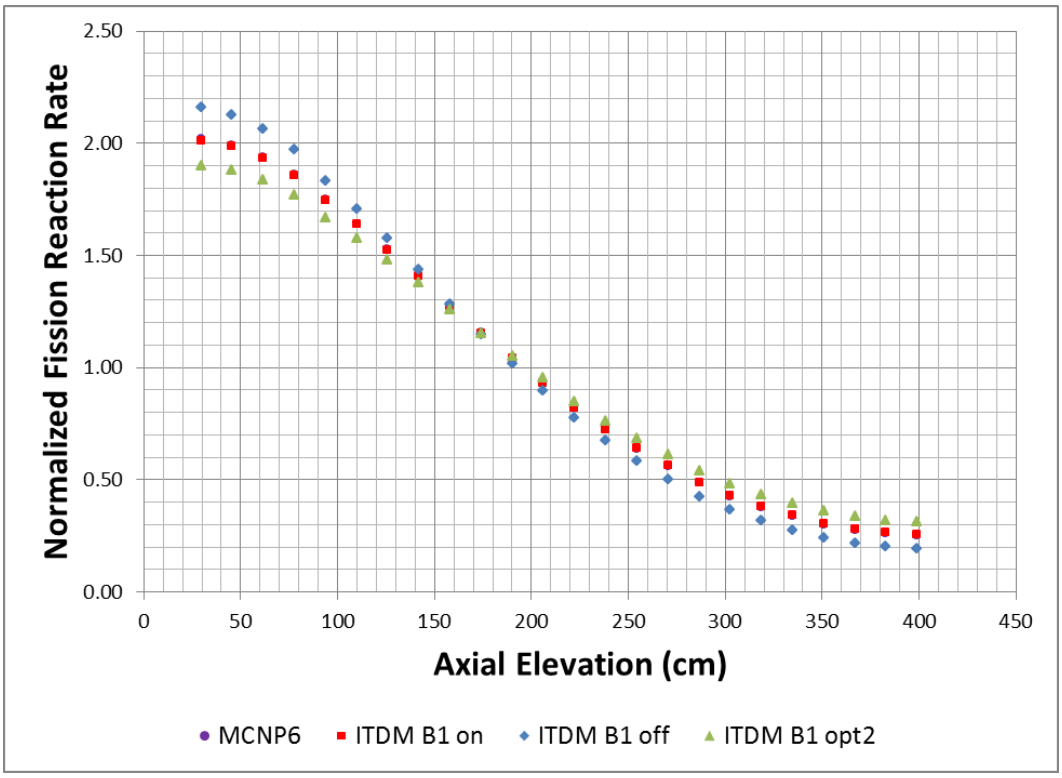

Figure 33: C3 ARO Core Average B1 Comparison

It can be seen that the B1 option used in ITDM has a significant impact on the axial reaction rate distribution. With the B1 option turned off, it can be seen that the tilt is slightly more significant, particularly in the UOX assemblies. Turning the B1 option on reduces the tilt, even reversing it in the UOX assemblies. Though a tilt still exists in each assembly, the averaged behavior of the core is predicted more accurately with B1 on. It is important to note that this is due to the offsetting of two axial tilts in opposite directions. Using opt2, it can be seen that the fission reaction rate tilt is biased toward the bottom of the core, similar to the B1 on distribution. This shows that the calculation method used for the diffusion coefficient does have a noticeable impact on the axial reaction rate distributions. The multiplication factors for each of the runs are shown below in Table 20.

Table 20: C3 ARO Core Average K_{eff} B1 Comparison

	K_{eff}	Difference (pcm)
MCNP6	1.17367	-
ITDM B1 on	1.17000	367
ITDM B1 off	1.17226	141
ITDM B1 opt2	1.17158	209

It is evident that the treatment of the B1 approximation and the diffusion coefficient is of great importance to the accuracy of the prediction. Above it can be seen that the B1 on option gives the closest axial reaction rate distributions to MCNP6, but a less accurate multiplication factor prediction. The B1 off option has the opposite effect, with opt2 falling in the middle.

Since such significant results were obtained, a rodded case (RA) of the C3 mini core was run at hot zero power (HZP) conditions in order to further examine the effects of the B1 approximation. The fuel and moderator properties throughout the entire length of the core were changed to those of the bottom layer from the previous calculations. The fuel and cladding temperatures were reduced to moderator temperature as well. Control rod material was inserted in the guide tube cells in layers 5 and 6 of the NW UOX assembly. The composition of the control rod material can be found in Table 21 below.

Table 21: Control Rod Material Composition

Element	Number Density [1/(b-cm)]
Boron-10	2.9833E-03
Carbon-12	3.7478E-03

The axial reaction rate distributions can be seen below in Figure 34, Figure 35, Figure 36 and Figure 37. The full results are tabulated in File 15 listed in Table 29. The NE and SW MOX assembly results are identical, so only NE is shown. However, the UOX assemblies now differ from each other due to the NW assembly being rodded.

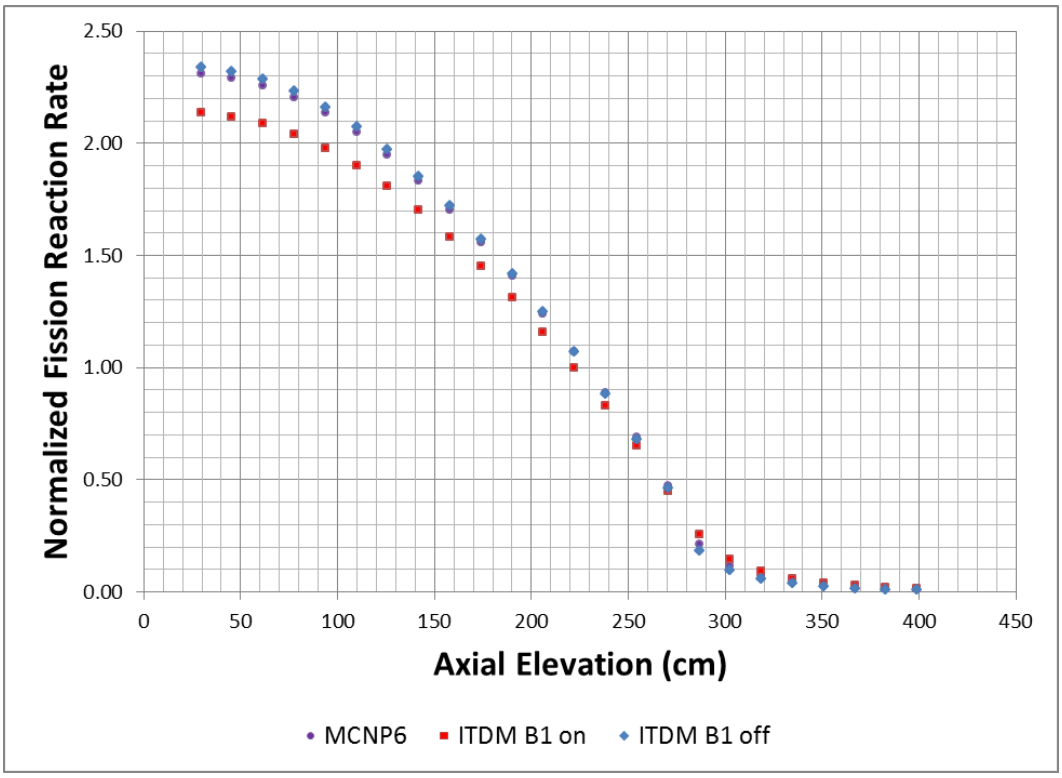

Figure 34: C3 RA HZP NW Rodded UOX Assembly B1 Comparison

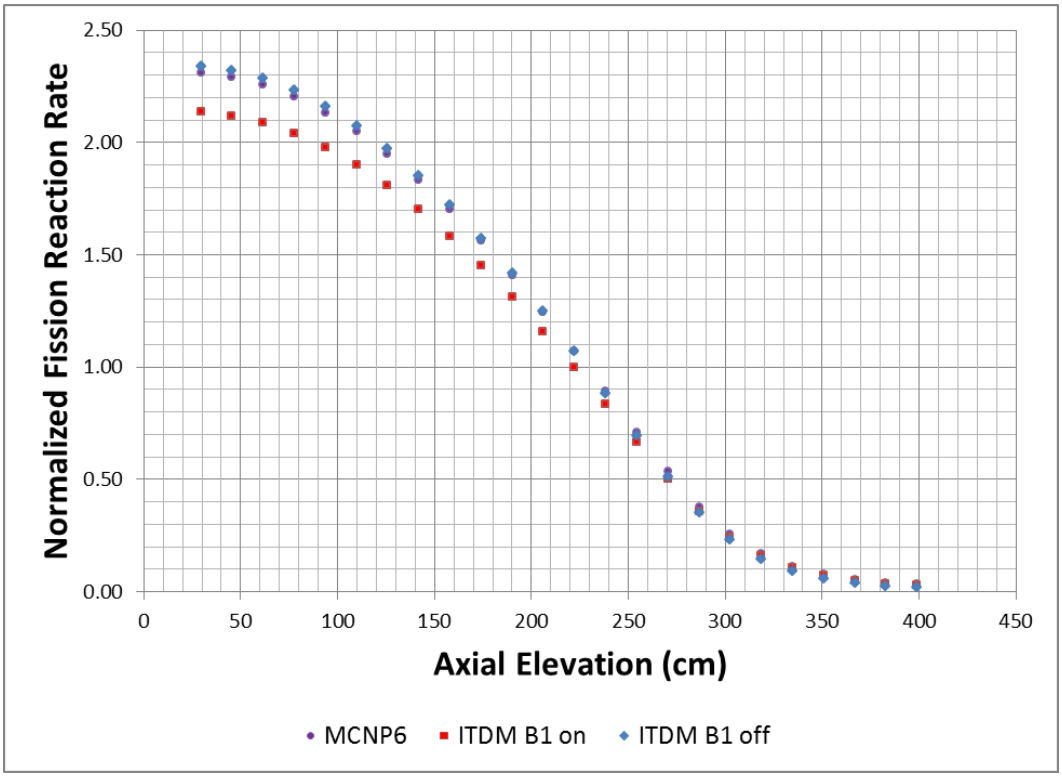

Figure 35: C3 RA HZP SE UOX Unrodded UOX Assembly B1 Comparison

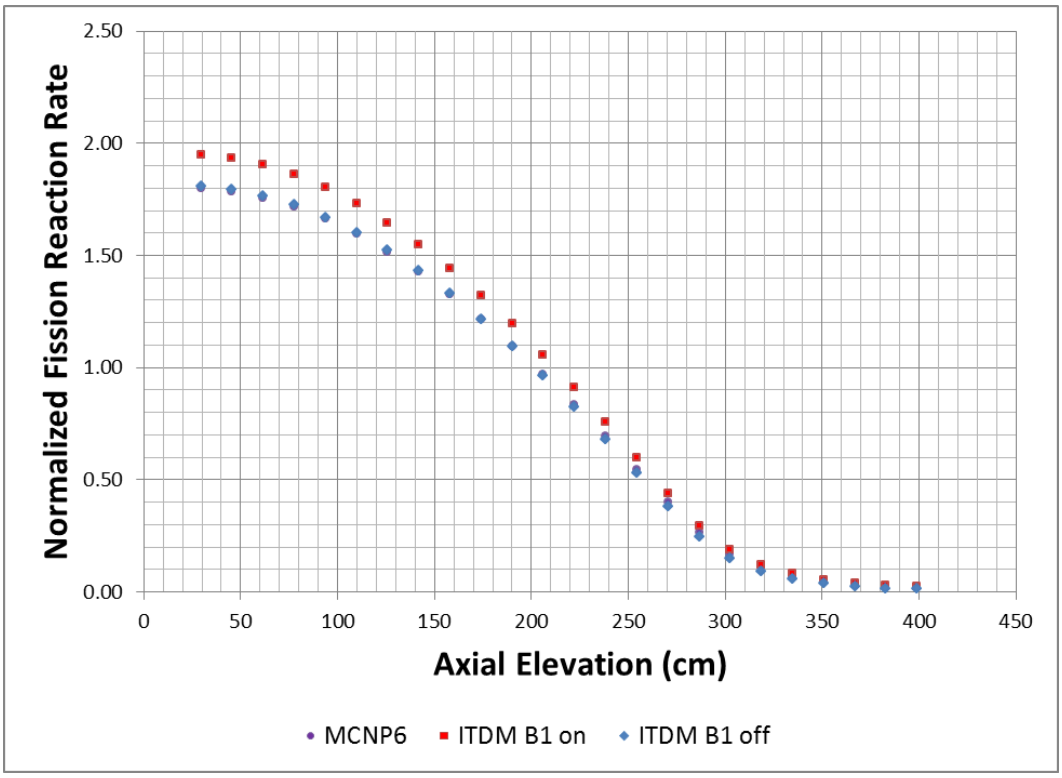

Figure 36: C3 RA HZP NE MOX Assembly B1 Comparison

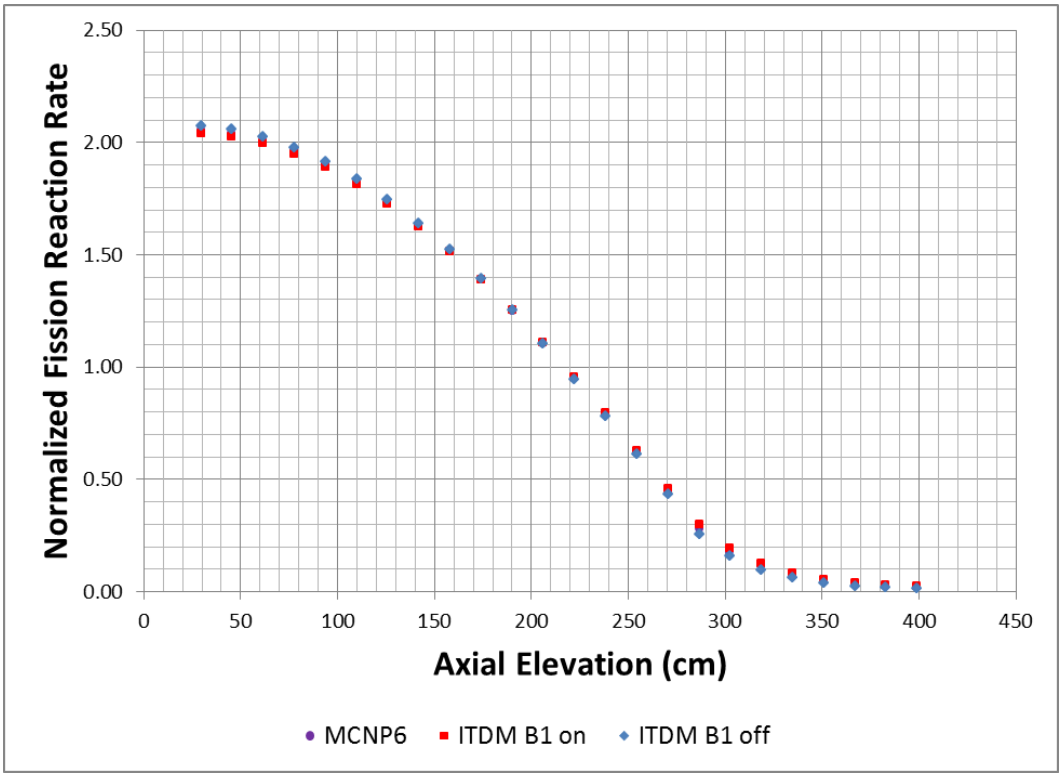

Figure 37: C3 RA HZP Core Average B1 Comparison

It can be seen that in the RA HZP case, the B1 approximation now has a detrimental effect on the axial fission reaction rate distributions. The B1 off case now shows a very minimal tilt in both uranium fueled assemblies. The mixed oxide fueled assemblies also show agreement between MCNP6 and ITDM B1 off. The multiplication factors are summarized in Table 22 below.

Table 22: C3 RA HZP Core K_{eff} B1 Comparison

	K_{eff}	Difference (pcm)
MCNP6	1.18838	-
ITDM B1 off	1.18800	38
ITDM B1 on	1.18493	345

It can be seen that the MCNP6 and ITDM B1 off runs have a difference of only 38 pcm. It is also seen that the B1 on case yields a much larger error. These results are seen further when examining the individual pin power errors seen below. Table 23 shows the absolute percent difference errors between MCNP6 and ITDM B1 off. Table 24 shows the same comparison for the B1 on option.

Table 23: C3 RA HZP Pin Power Errors MCNP6 vs. ITDM B1 off

Abs. % Diff	NW UOX	SE UOX	NE MOX	SW MOX
Core Max	4.63%	4.74%	6.38%	5.95%
Core Min	-4.83%	-3.59%	-3.95%	-3.87%
Core Avg	1.55%	1.85%	1.36%	1.36%
Max Layer RMS	3.02%	2.96%	2.10%	2.12%
Min Layer RMS	0.38%	0.51%	0.72%	0.75%
Avg Layer RMS	1.62%	1.92%	1.55%	1.54%

Table 24: C3 RA HZP Pin Power Errors MCNP6 vs. ITDM B1 on

Abs. % Diff	NW UOX	SE UOX	NE MOX	SW MOX
Core Max	11.27%	0.24%	19.40%	19.41%
Core Min	-28.31%	-28.65%	-0.04%	-0.06%
Core Avg	8.24%	8.09%	7.66%	7.66%
Max Layer RMS	18.02%	17.87%	14.94%	14.84%
Min Layer RMS	0.33%	0.23%	0.22%	0.19%
Avg Layer RMS	8.47%	8.31%	7.72%	7.72%

When comparing the two cases, it can be seen that the B1 off option has much lower errors than the B1 on option. Agreement between MCNP6 and the B1 off case is actually quite reasonable with average layer RMS errors of less than 2%, while the B1 on case presents much larger errors throughout.

The results of this section seem to be somewhat contradictory when examining both the C3 RA HZP and C3 ARO HFP cases. It seems that the B1 approximation has a significant impact on the axial reaction rate distribution and the pin powers. In the HFP case it seemed to help, but in the rodded HZP case, it added greatly to the error. Again, it should be noted that in the HFP B1 on case that the tilts seen in the individual assemblies offset each other to yield a more accurate core average distribution.

Due to these results, it was determined that the B1 approximation should not be used in the simulation. It cannot be overlooked that the B1 approximation has a great impact on both the axial fission reaction rate distribution and the multiplication factor, though. However, it was hypothesized that the significant changes in the results were more likely due to the B1 approximation's effective simulation of axial neutron transference and also the differences in the calculation of the diffusion coefficients. Therefore, it was decided that the axial transference and diffusion coefficients should be further investigated.

5.4 Axial Leakage Study

Since the B1 approximation has such a significant impact on the results, it is hypothesized that the cause of the tilt may be rooted in the modelling of the axial transference of neutrons between layers. Therefore, a study on the effects of inter-layer axial leakage in ITDM was performed. To this point, leakage of neutrons between layers was not simulated; it was only approximated using the B1 option.

The C3 ARO mini core was simulated with and without inter-layer axial leakage to observe the results. The B1 approximation was left off and the diffusion coefficients were calculated using the standard diffusion approximation after collapsing the transport cross sections. Below, in Figure 38, Figure 39, and Figure 40, the results are presented. These results are tabulated in File 9 listed in Table 29. It can be seen that the treatment of axial leakage of neutrons has made a minimal improvement to the axial fission reaction rate distribution in each assembly, as well as the core averaged distribution.

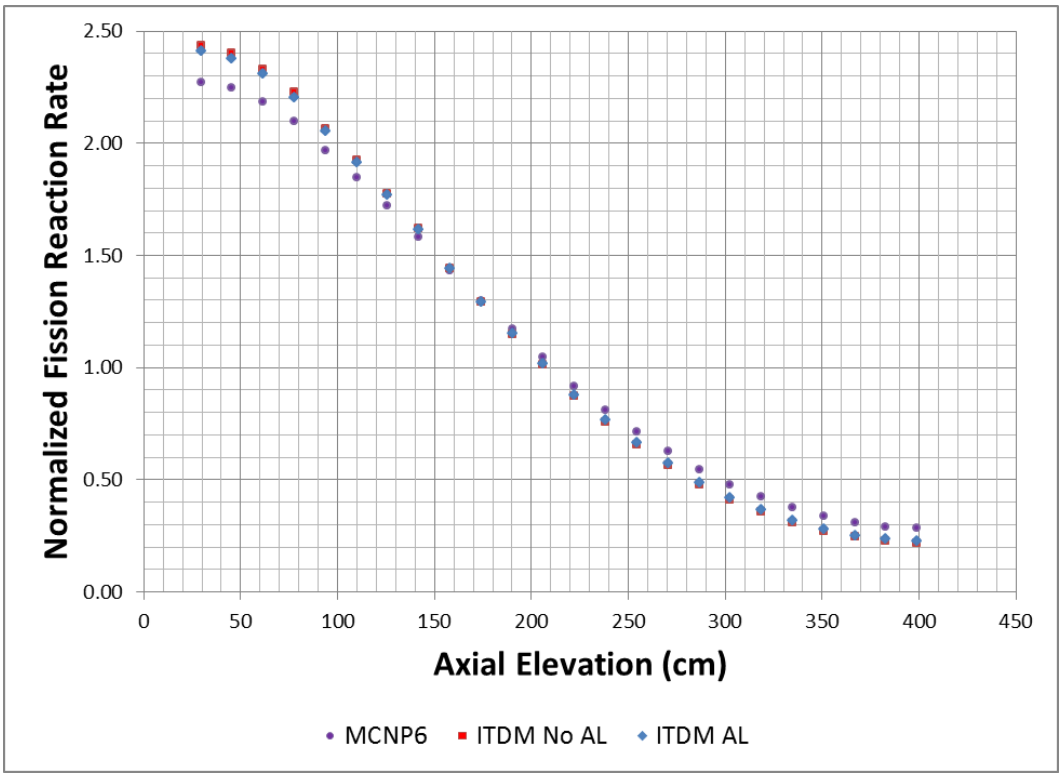

Figure 38: C3 ARO NW UOX Inter-Layer Axial Leakage Comparison

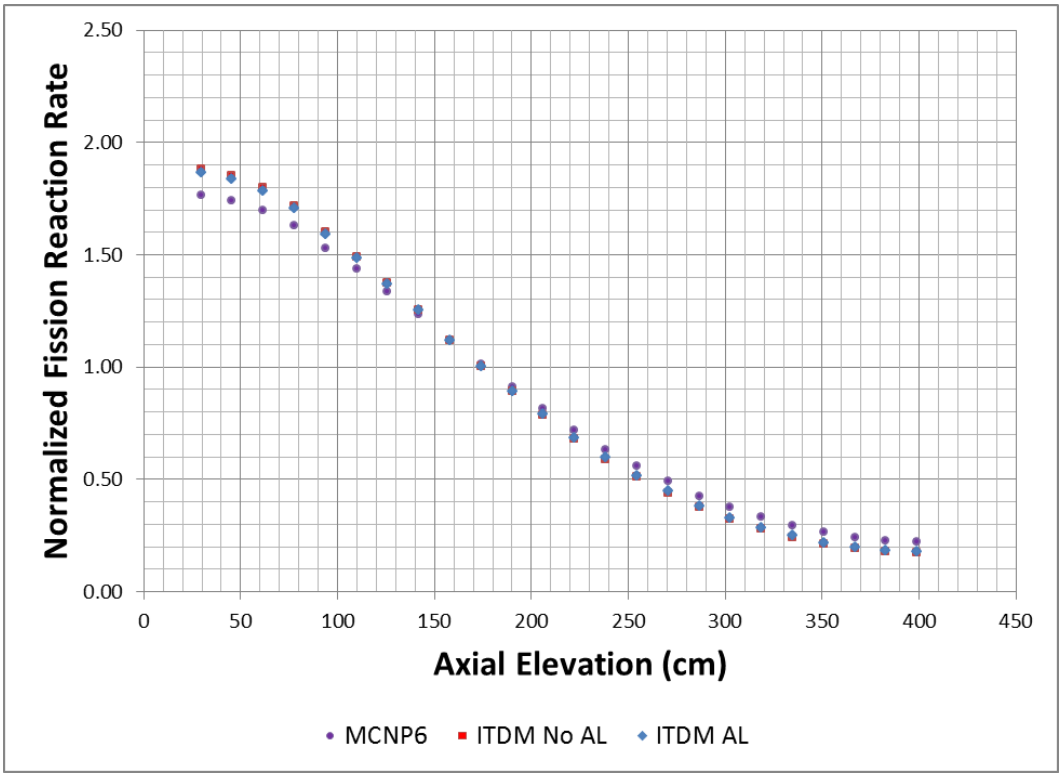

Figure 39: C3 ARO NE MOX Inter-Layer Axial Leakage Comparison

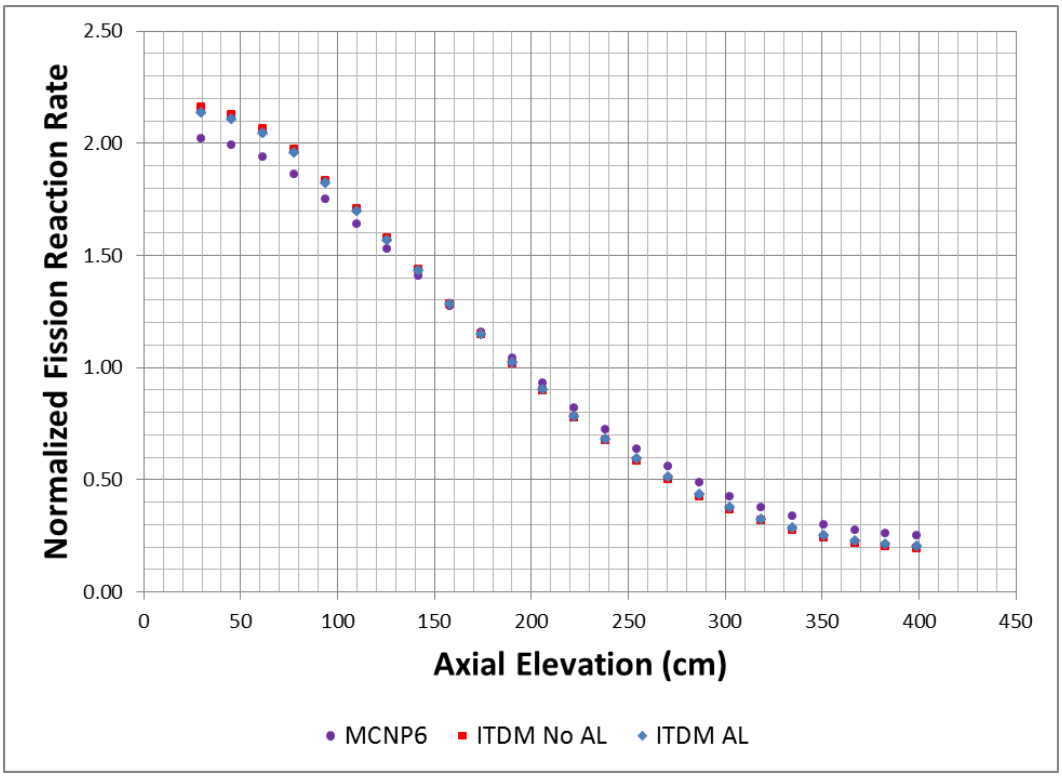

Figure 40: C3 ARO Core Average Inter-layer Axial Leakage Comparison

Below, in Table 25, the multiplication factors for each run are summarized. It can be seen that the prediction of the multiplication factor is decreased slightly, further from the MCNP6 prediction.

Table 25: C3 ARO Core Average K_{eff} Inter-Layer Axial Leakage Comparison

	K_{eff}	Difference (pcm)
MCNP6	1.17367	-
ITDM No AL	1.17226	141
ITDM AL	1.17210	157

A comparison of pin power errors for each of the runs can be seen below in Table 26 and Table 27. These comparisons are tabulated in Files 10 and 12 listed in Table 29.

Table 26: C3 ARO Pin Power Errors MCNP6 vs. ITDM No AL

Abs. % Diff	NW UOX	SE UOX	NE MOX	SW MOX
Core Max	21.50%	21.92%	16.12%	15.70%
Core Min	-8.62%	-8.73%	-6.87%	-6.84%
Core Avg	7.03%	7.02%	5.24%	5.25%
Max Layer RMS	16.63%	16.56%	11.64%	11.56%
Min Layer RMS	0.77%	0.93%	0.91%	0.97%
Avg Layer RMS	7.16%	7.15%	5.34%	5.35%

Table 27: C3 ARO Pin Power Errors MCNP6 vs. ITDM AL

Abs. % Diff	NW UOX	SE UOX	NE MOX	SW MOX
Core Max	16.97%	16.64%	15.99%	15.66%
Core Min	-7.39%	-7.40%	-6.06%	-6.10%
Core Avg	5.98%	5.97%	4.61%	4.62%
Max Layer RMS	13.83%	13.76%	10.42%	10.33%
Min Layer RMS	0.64%	0.82%	1.10%	1.16%
Avg Layer RMS	6.06%	6.05%	4.77%	4.78%

It can be seen that the MOX assemblies show only miniscule improvement in the pin errors when the axial leakage is accounted for. However, the errors decrease more noticeably in the UOX assemblies when the axial leakage is used.

The improvements seen using 24 axial layers with axial leakage simulated suggest that an axial mesh refinement, such as the one from the NEM discretization study section, may prove to further benefit the results. Therefore, smaller mesh sizes in NEM were run with the axial leakage option to determine if the axial leakage simulation would improve. The results are shown below in Figure 41, Figure 42, and Figure 43 and are tabulated in File 13 listed in Table 29. It can be seen that the axial reaction rate distribution obtained using axial leakage with increased NEM

discretization has not changed in the UOX assemblies and shows minimal decrease in accuracy in the MOX assemblies. The multiplication factor prediction also shows an increase in error, seen in Table 28.

Table 28: C3 ARO Core Average K_{eff} Axial Leakage NEM Discretization Comparison

	K_{eff}	Difference (pcm)
MCNP	1.17367	-
ITDM 1NPA 24 Layers No AL	1.17226	141
ITDM PxP 96 Layers AL	1.16813	554

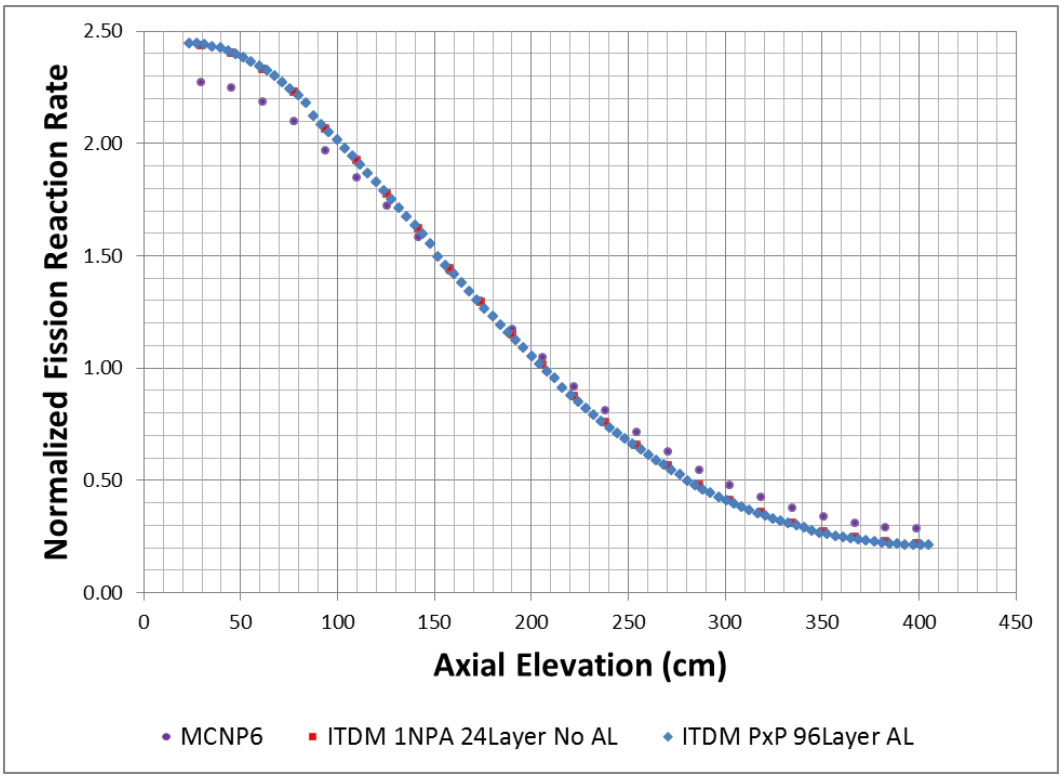

Figure 41: C3 ARO NW UOX Assembly Axial Leakage with NEM Discretization

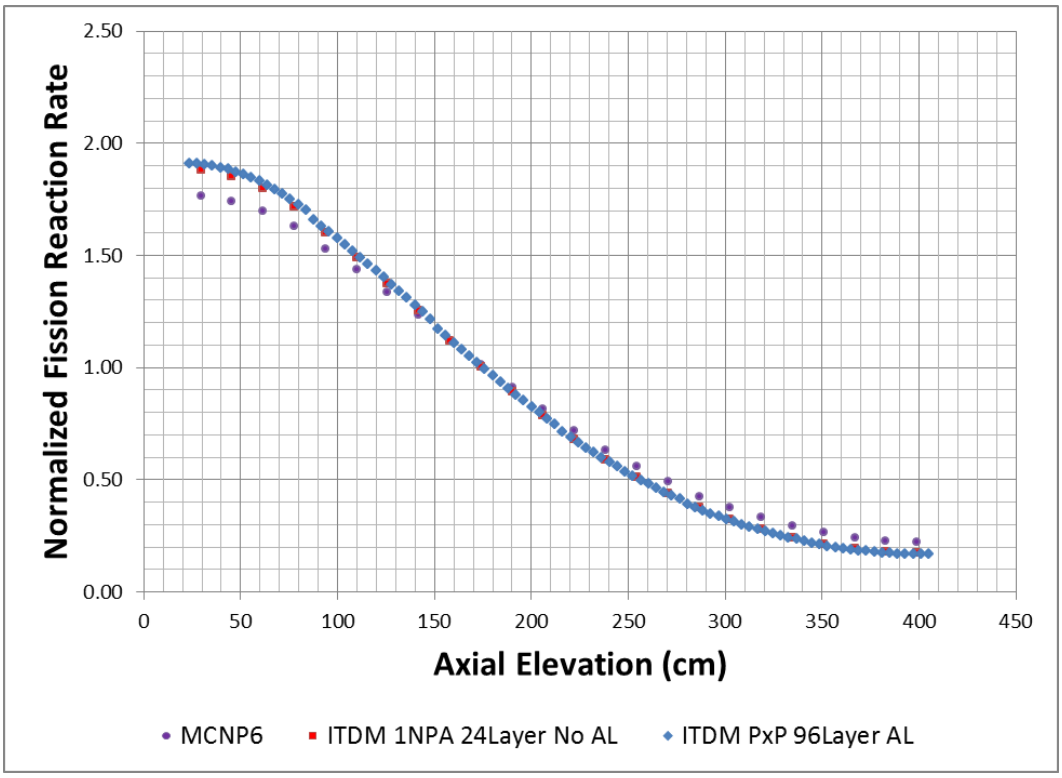

Figure 42: C3 ARO NE MOX Assembly Axial Leakage with NEM Discretization

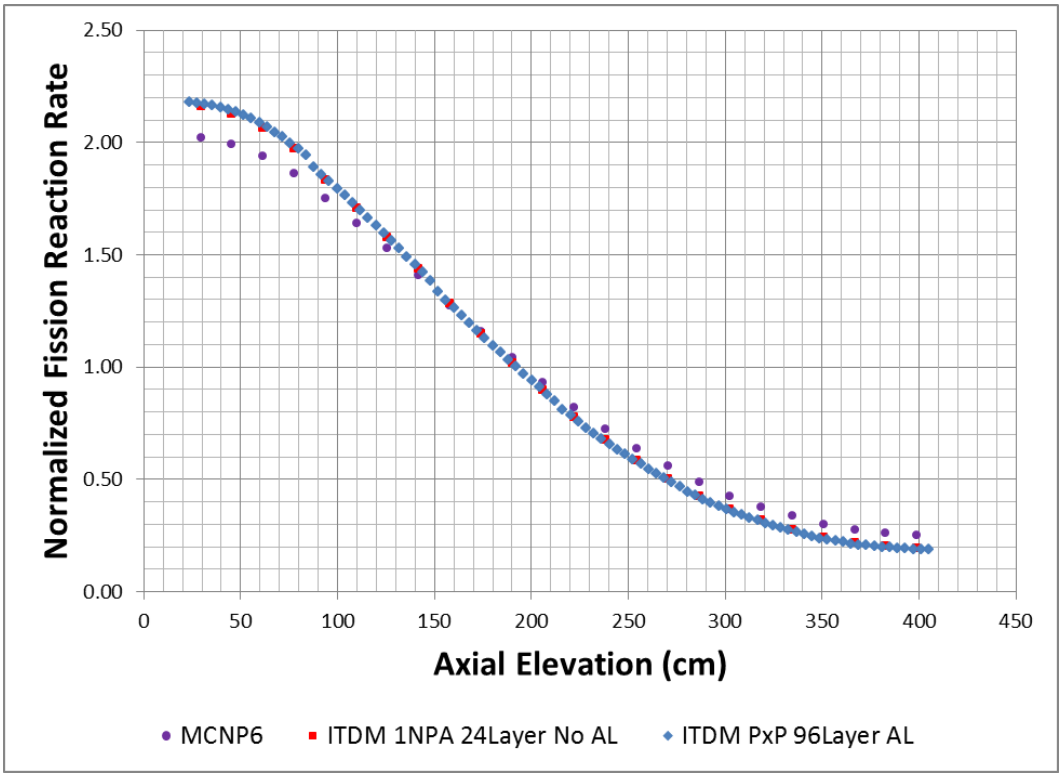

Figure 43: C3 ARO Core Average Axial Leakage with NEM Discretization

These results show that the axial leakage treatment of neutrons does in fact have an effect on the results. However, the fact that improvement was seen in the 24 axial layer case, but not in the 96 axial layer case, suggests that there may be an issue with the implementation of the axial leakage treatment in ITDM and that it should be investigated further.

5.5 Axial Leakage Energy Reconstruction

Upon investigation, it was discovered that the energy treatment in the axial leakage source terms was oversimplified in its original implementation. The axial leakage source term is calculated using the NEM generated net neutron current at both the top and bottom surfaces of each axial layer for each pin. These net leakages are summed to provide a cell averaged net axial leakage source. When this value is calculated, the information is in terms of the NEM macro energy groups. However, PARAGON requires fine group information for its axial leakage sources. Therefore, in original implementation, the macro group net leakage sources were simply divided by the number of micro groups contained in the macro group of interest. However, this approximation is not physically correct and may be causing the inconsistent results seen between the 24 and 96 layer runs in the previous section.

Therefore, a new procedure is currently being implemented in the ITDM code. In this procedure, the PARAGON output is formatted to print information for all micro groups in the calculation. Previously, PARAGON ran using the micro groups in its collision probability scheme, and then collapsed the information to the specified macro group structure before printing the output. Now, PARAGON will not collapse the information. Instead, ITDM will read all of the micro group information from PARAGON and do the collapsing itself in a new subroutine. This will allow ITDM to retain the micro group energy structures, which can then be used to reconstruct the axial leakage sources more correctly. The collapsing for each of the parameters in ITDM is computed in the same way as PARAGON would do internally.

First, the fluxes, currents, and fission spectra are simply summed according to equation (5.1) below. In this equation, X represents the parameter of interest, g represents the micro group number, and G represents the macro group number.

$$X_G = \sum_G X_g \,, \qquad g \in G \tag{5.1}$$

Next, the cross sections and diffusion coefficients are flux averaged as shown below in equation (5.2). In this equation the variables are the same as in equation 1 with the addition of the volumetric flux, represented by ϕ. It should be noted that the scattering cross section matrix is flux averaged, but the procedure differs slightly from equation (5.2) because of the extra energy group dependence associated with the transference of neutrons from the micro group of interest to each other micro group.

$$X_G = \frac{1}{\emptyset_G} \sum_G X_g \emptyset_g \,, \qquad g \in G \tag{5.2}$$

The energy per fission is then collapsed using a fission reaction rate average. This is shown below in equation (5.3) where E represents the energy per fission, and Σ_f is the macroscopic fission cross section. The other variables remain the same as in equations (5.1) and (5.2).

$$E_G = \frac{\sum_G E_g \emptyset_g \Sigma_{f,g}}{\sum_G \phi_g \Sigma_{f,g}}, \qquad g \in G \tag{5.3}$$

In addition to collapsing the above information, the albedos need to be recalculated. They are as follows, in equation (5.4).

$$Albedo_G = \frac{\sum_G J_{in_g}}{\sum_G J_{out_g}}, \qquad g \in G \tag{5.4}$$

ITDM will now retain the micro group energy structure and it will no longer be lost in the PARAGON collapsing scheme. Thus, the pin-wise flux energy shape can be reconstructed from iteration to iteration, hopefully leading to an improvement in the accuracy of the axial leakage treatment.

5.6 Diffusion Coefficient Energy Collapsing

Another benefit realized by obtaining the micro group information is in the calculation of the diffusion coefficients in ITDM. Previously, it was only possible to calculate the diffusion coefficient after the transport cross sections were collapsed as seen in equation (5.5).

$$D_G = \frac{1}{3\Sigma_{tr_G}} \tag{5.5}$$

However, with the new capabilities it will be possible to collapse the diffusion coefficient after calculation. This formulation of the diffusion coefficient, shown in equation (5.6) below, is the basis for many codes used today such as SIMULATE. (Lamarsh & Baratta, 2001)

$$D_G = \frac{1}{3\phi_G}\sum_G \frac{1}{\Sigma_{tr_g}}\phi_g\,, \qquad g \in G \tag{5.6}$$

It is hypothesized that this change in the calculation of the diffusion coefficient will lead to significantly improved results. This is because the diffusion coefficient is such an important parameter in diffusion theory, which is used by NEM. Since NEM is greatly responsible for the axial treatment of the simulation, an improved calculation method for the diffusion coefficient should affect the axial distribution directly.

CHAPTER 6
CONCLUSIONS AND FUTURE WORK

6.1 Conclusions

In the continuation of the Next Generation Method (NGM) Iterative Transport-Diffusion Methodology (ITDM) project, the previously obtained results were successfully reproduced. The Monte Carlo N-Particle (MCNP) reference was updated to include more realistic moderator properties including temperature, density, and chemical composition. These changes in the moderator were also implemented in the ITDM simulation. It was found that the axial tilt previously seen remained after these updates. Many sensitivity studies were performed in order to isolate the cause of the tilt seen in the results.

It was found that changing the nodal discretization in the radial and axial directions in the Nodal Expansion Method (NEM) portion of ITDM had negligible effects on the axial fission reaction rate distributions. Small changes were seen in the multiplication factor prediction when the number of axial nodes was increased. However, agreement worsened with larger numbers of layers and the increased number of layers dramatically increased the runtime for the ITDM program. In the radial direction, it was seen that the pin by pin calculation also worsened the multiplication factor prediction and increased runtime.

Upon examining the level of radial discretization in the 2-D transport solver, PARAGON, similar results were seen for the axial fission reaction rate distributions. Differences were negligible. However, the multiplication factor predictions were slightly improved with each level of increased discretization. It should be noted that these changes in k_{eff} are relatively small, but the difference in runtime is quite significant.

The B1 approximation option in ITDM was found to have a significant impact on the axial fission reaction rate distributions, even reversing the direction of the axial tilt in some cases. It was found that the un-rodded hot full power (HFP) simulations using the B1 approximation yielded slightly more accurate axial reaction rate distributions than those without the B1 approximation. However, the multiplication factor was more closely predicted without the B1 approximation. The opt2 simulations were found to be approximately in the middle of the other two options in both comparisons. Although there were changes observed due to the B1 approximation, an axial tilt was still seen in each assembly for each case, some biased in different directions than others.

Somewhat contradictory results were obtained when examining a rodded hot zero power (HZP) core. In this case, the B1 approximation produced a significant axial tilt in each assembly. The ITDM simulation that did not use the B1 approximation was found to be much more accurate and produced a very minimal tilt in only the uranium oxide (UOX) assemblies. The multiplication factor was predicted with a difference of only 38 pcm with the B1 option turned off. With B1 on, the error multiplied. Due to the nature of the B1 approximation and its impact on the results, it was hypothesized that the tilt may be related to the treatment of the inter-layer transference of neutrons and the calculation of the diffusion coefficients.

Inter-layer axial leakage was then simulated in ITDM. The results showed little to no change caused by the axial leakage option in the axial fission reaction rate distributions. However, it was observed that the axial leakage simulations yielded slightly less accurate multiplication factors. It was also found that an increase in NEM axial discretization did not help the axial leakage simulation. In fact, it was found that pin by pin runs with and 96 layers and axial leakage were slightly worse than those using one node per assembly with 24 layers and no

axial leakage. These results may be due to the energy treatment of the axial leakage sources in the ITDM code.

Upon initial implementation of the axial leakage treatment, the energy spectra were oversimplified. This issue is currently being corrected. In correcting this issue, it will also be possible to calculate the diffusion coefficient prior to collapsing the transport cross sections. It is hoped that this more conventional way of calculating the diffusion coefficient will lead to more accurate modelling in NEM, and thus a more accurate axial solution.

6.2 Future Work

In Dr. Colameco's thesis, it is hypothesized that the axial tilt may be affected by the use of the polynomial expansion in NEM. It is strongly suggested that a semi-analytical version of NEM be substituted. Therefore, semi-analytical NEM has been obtained, though it has not yet been implemented. It should be implemented in the ITDM code to examine its effects on the results.

Work toward correcting the axial tilt in the fission reaction rate distribution should continue until it is corrected. It is hoped that the improved energy treatment and calculation of the diffusion coefficient before collapsing will remedy the tilt. Once corrected, additional rodded C3 cases may be simulated as well as rodded and un-rodded C5 cases. These cases should also be examined on the pin level for inconsistencies. In these C5 cases, it is likely that reflector convergence issues may arise. These issues should also be investigated.

APPENDIX A List of Files

This appendix will serve as a guide to the accompanying files used to run MCNP and ITDM and to produce the output seen in this report. Table 29 below lists the accompanying files and folders included in the ITDM_Update_2014.tar file.

Table 29: Accompanying Files

File #	File Name and Location	Description
1	/Input_Files/ITDM/prgnem.in_1NPA_24Layers	Sample 24 Layer ITDM Input File
2	/Input_Files/ITDM/prgnem.in_1NPA_48Layers	Sample 48 Layer ITDM Input File
3	/Input_Files/ITDM/prgnem.in_1NPA_96Layers	Sample 96 Layer ITDM Input File
4	/Input_Files/ITDM/prgnem.in_289NPA	Sample PxP ITDM Input File
5	/Input_Files/ITDM/prgnem.in_RA_HZP	Sample RA HZP ITDM Input File
6	/Input_Files/MCNP/C3_ARO_NE_HFP	Sample C3 ARO HFP MCNP Input File
7	/Input_Files/MCNP/C3_RA_NE_HZP	Sample C3 RA HZP MCNP Input File
8	/Input_Files/MCNP/In_C2_ARO_NE_L1AP1	Sample Non-updated MCNP Input File for Custom Library
9	/Results/Axial_Leakage_Study_B1off.xlsx	Results for Axial Leakage Study B1 Off with Plots
10	/Results/Axial_Leakage_Study_B1off_Pin_Errors.xlsx	Results for Axial Leakage Study B1 Off with Pin Power Comparisons
11	/Results/Axial_Leakage_Study_B1on.xlsx	Results for Axial Leakage Study B1 On with Plots
12	/Results/Axial_Leakage_Study_B1on_Pin_Errors.xlsx	Results for Axial Leakage Study B1 On with Pin Power Comparisons
13	/Results/Axial_Leakage_Study_NEM_Discretization.xlsx	Results for Axial Leakage Study with Nem Discretization
14	/Results/B1_Approximation_Study.xlsx	Results for B1 Approximation Study
15	/Results/B1_RA_HZP_Study.xlsx	Results of B1 RA HZP Study with Plots and Pin Errors
16	/Results/MCNP_Temperature_Update.xlsx	Results of MCNP Temperature Update with Plots
17	/Results/Moderator_Density_Update.xlsx	Results of Moderator Density Update with Plots
18	/Results/NEM_Discretization_Study.xlsx	Results of NEM Discretization Study with Plots
19	/Results/NEM_Discretization_Study_Pin_Errors.xlsx	Results of NEM Discretization Study with Pin Power Comparisons
20	/Results/PRGN_Discretization_Study.xlsx	Results of PRGN Discretization Study with Plots
21	/Results/PRGN_Discretization_Study_Pin_Errors.xlsx	Results of PRGN Discretization Study with Pin Power Comparisons

22	/Scripts/grep_MCNP_Data.txt	Shell Script Extracts Pin Data from MCNP for Excel Files
23	/Scripts/PRGNEMgrep_24.txt	Shell Script Combines Assembly Data from Final Iteration of ITDM with 24 Layers
24	/Scripts/PRGNEMgrep_48.txt	Shell Script Combines Assembly Data from Final Iteration of ITDM with 48 Layers
25	/Scripts/PRGNEMgrep_96.txt	Shell Script Combines Assembly Data from Final Iteration of ITDM with 96 Layers
26	/Scripts/Run_MCNP_C3_ARO_NE	Sample Shell Script Used to Qsub MCNP Run to PBS Queue on HPC
27	/Scripts/Run_Script_prgnem	Sample Shell Script Used to Qsub ITDM Run to PBS Queue on HPC
28	/Supporting_Files/ITDM_First_Cycle_Input/High_Discretization/	Folder Containing First Cycle PARAGON Input Files with High Discretization
29	/Supporting_Files/ITDM_First_Cycle_Input/Low_Discretization/	Folder Containing First Cycle PARAGON Input Files with Low Discretization
30	/Supporting_Files/ITDM_First_Cycle_Input/No_Discretization/	Folder Containing First Cycle PARAGON Input Files with No Discretization
31	/Supporting_Files/ITDM_First_Cycle_Input/RA_HZP/	Folder Containing First Cycle PARAGON Input Files for RA HZP Cases
32	/Supporting_Files/MCNP_mT_broad/	Folder Containing Broadened Moderator Chemical Compound Cross Section Files
33	/Supporting_Files/MCNP_OTF/	Folder Containing Temperature adjusted OTF Cross Section Files
34	/Supporting_Files/MCNP_XSEC/	Folder Containing Custom 70-Group MCNP5 Libraries and Directory
35	/Supporting_Files/Paragon_Library/prgnlib.124	PARAGON Cross Section Library Used for ITDM Runs

APPENDIX B Results Instructions

Extracting ITDM results for use in Excel files:

1. Open the prgnem.out file.
2. Copy all of the blocks listed under "Core Normalized Fission Reaction Rate distribution for FType:" for the final (converged) iteration and paste these into a file named finaliteration.out.
3. Put the finaliteration.out and the appropriate PRGNEMgrep_*.txt file (File number 23, 24 or 25) for the number of layers run in the same directory and run the .txt file.
4. A file for each cardinal direction will be produced. The contents of this file can then be copied and pasted into cell A1 on the corresponding sheet in the Excel workbook. These sheets are named PRGNEM*NW depending on the case and cardinal direction of the assembly. The *_Calcs sheets should not need to be edited.
5. After pasting, press ctrl and select Use Text Import Wizard… Click finish, then Ok.

Extracting MCNP results for use in Excel Files:

1. Ensure that the MCNP output file name ends with .out. Each of the 4 assemblies uses a separate file and MCNP run.
2. Place File 22 in the same directory as the output file and run it.
3. A new file will be created with the results for that assembly. The contents of this file can be copied and pasted into cell A1 of the appropriate sheet in the Excel workbook. These sheets are named MCNP*NW depending on the case and cardinal direction of the assembly. The *_Calcs sheets should not need to be edited.
4. Follow step 5 from the section above.

Once the data is correctly pasted in the excel workbook, all of the plots and calculations should update to give the desired results and comparisons. In the Pin Error files, the *_Calcs pages have been updated to *_Calcs_Pin Errors and make a pin by pin comparison with the directly preceding (tabs to the left) MCNP results. The MCNP6 results are repeated in many of these files because of this and are listed under MCNP2* or MCNP3* rather than MCNP6*. These results are all the same.

REFERENCES

Colameco, D. (2012). Next Generation Iterative Transport-Diffusion Methodology (ITDM) for LWR Core Analysis. *Pennsylvania State University, Doctoral Dissertation in Nuclear Engineering*.

Colameco, D., Ivanov, B. D., Beacon, D., & Ivanov, K. N. (2013). Iterative Transport-Diffusion Methodology for LWR Core Analysis. Paper # 164, Paris, France: SNA + MC 2013.

Collins, B., Kochunas, B., & Downar, T. (2013). Assessment of the 2D MOC Solver in MPACT: Michigan Parallel Characteristics Transport Code. Paper # 8071, Sun Valley, ID: American Nuclear Society.

Fevotte, F., & Lathuiliere, B. (2013). MICADO : Parallel Implementation of a 2D–1D Iterative Algorithm for the 3D Neutron Transport Problem in Prismatic Geometries. Paper # 7288, Sun Valley, ID: American Nuclear Society.

Hou, J., Ivanov, K., & Choi , H. (2014). Development of an Iterative Lattice-Core Coupling Method Based on MICROX-2 Cross Section Libraries. Paper # 1104814, Kyoto, Japan: Physor 2014.

Ivanov, B. D. (2007). Methodology for Embedded Transport Core Calculation. *Pennsylvania State University, Doctoral Dissertation in Nuclear Engineering*.

Jung, Y. S., Joo, H. G., & Yoon, J. I. (2013). Core Follow Calculation with the nTRACER Numerical Reactor and Verification Using Power Reactor Measurement Data. Paper # 7817, Sun Valley, ID: American Nuclear Society.

Karriem, Z., Ivanov, K., Rabiti, C., & Gougar, H. (2014). The Development and Testing of the HELIOS-2 Lattice Code for Use In On-Line Cross-Section Generation. *International Conference on Mathematics and Computational Methods Applied to Nuclear Science & Engineering (M&C 2013).* Paper # 7341, Sun Valley, Idaho, USA, May 5-9, 2013.

Kelley, B. W., & Larsen, E. W. (2013). 2D/1D Approximations to the 3D Neutron Transport Equation. I: Theory. Paper # 8058, Sun Valley, ID: American Nuclear Society.

Kelley, B. W., Collins, B., & Larsen, E. W. (2013). 2D/1D Approximations to the 3D Neutron Transport Equation. II: Numerical Comparisons. Paper # 8060, Sun Valley, ID: American Nuclear Society.

Kochunas, B., & Downar, T. J. (2013). Parallel 3-D Method of Characteristics in MPACT. Paper # 8058, Sun Valley, ID: American Nuclear Society.

Kochunas, B., Collins, B., Jabaay, D., Downar, T. J., & Martin, W. R. (2013). Overview of Development and Design of MPACT: Michigan Parallel Characteristics Transport Code. Paper # 8060, Sun Valley, ID: American Nuclear Society.

Lamarsh, J. R., & Baratta, A. J. (2001). *Introduction to Nuclear Engineering.* Upper Saddle River, NJ: Prentice-Hall, Inc.

Lee, G. S., & Cho, N. Z. (2006). 2D/1D fusion method solutions of the three-dimensional transport OECD benchmark problem C5G7 MOX. *Progress in Nuclear Energy*, Volume 48, Issue 5, Pages 410-423

Lewis, E. E., & Miller, W. F. (1993). *Computational Methods of Neutron Transport.* La Grange Park, IL: American Nuclear Society.

Liu, Z., Kochunas, B., Collins, B., Downar, T., & Wu, H. (2013). The Method of Modular Characteristic Direction Probabilities in MPACT. Paper # 7922, Sun Valley, ID: American Nuclear Society.

Martin, W. R., Wilderman, S., Brown, F. B., & Yesilyurt, G. (2013). Implementation of On-the-Fly Doppler Broadening in MCNP. Paper # 7903, Sun Valley, ID: American Nuclear Society.

RDFMG. (2009). *NEM Theory Manual.* University Park, PA: Department of Mechanical and Nuclear Engineering.

Roberts, D. R. (2010). Development of Iterative Transport-Diffusion Methodology for LWR Analysis. *Pennsylvania State University, Master's Thesis in Nuclear Engineering*.

Stimpson, S., Young, M., Collins, B., Kelley, B., & Downar, T. (2013). Assessment and Improvement of the 2D/1D Method Stability in DeCART. Paper # 8024, Sun Valley, ID: American Nuclear Society.

Takeda, T., Fujita, Y., Kitada, T., Yamaji, K., & Matsumoto, H. (2009). Hybrid Method of MOC and S_N Nodal for PWR Core Analysis. *International Conference on Mathematics, Computational Methods & Reactor Physics (M&C 2009).* Paper # 356, Saratoga Springs, NY: American Nuclear Society.

X-5 Monte Carlo Team. (2003). *MCNP — A General Monte Carlo N-Particle Transport Code, Version 5 Volume I: Overview and Theory.* Los Alamos, NM: Los Alamos National Laboratory.

Zhang, H., Zheng, Y., Wu, H., & Cao, L. (2013). A 2D/1D Coupling Neutron Transport Method Based on the Matrix MOC and NEM Methods. Paper # 7216, Sun Valley, ID: American Nuclear Society.